

1 **Tropical Sea Surface Temperatures following the Middle Miocene Climate Transition from Laser-**
2 **Ablation ICP-MS analysis of glassy foraminifera**

3

4 **Michael G. Nairn¹, Caroline H. Lear¹, Sindia M. Sosdian¹, Trevor R Bailey², and Simon**
5 **Beavington-Penney³**

6 ¹School of Earth and Ocean Sciences, Cardiff University, Cardiff, UK, ²Department of Natural
7 Sciences, Amgueddfa Cymru, National Museum Wales, Cathays Park, Cardiff, ³ BG Group, 100
8 Thames Valley Park Drive, Reading, RG6 1PT, UK*

9

10 Corresponding author: Michael G. Nairn (NairnMG@cardiff.ac.uk)

11

12 *Current address: Department of Earth and Environmental Sciences, The University of
13 Manchester, Williamson Building, Oxford Road, Manchester, M13 9PL, UK

14

15 **Key Points:**

- 16 • Laser-Ablation ICP-MS facilitates absolute sea surface temperature reconstructions using
17 foraminifera with diagenetic coatings.
- 18 • Tropical sea surface temperatures remained relatively stable at 24-31°C following the
19 Miocene Climate Transition.
- 20 • An increased latitudinal temperature gradient developed through the mid-to-late Miocene.

21

22

23 Abstract

24 The unipolar icehouse world of the mid-late Miocene is a poorly understood interval in the
25 evolution of Cenozoic climate, and the sparse proxy-based climate reconstructions are associated
26 with large uncertainties. In particular, tropical sea surface temperature (SST) estimates largely
27 rely on the unsaturated alkenone U_{37}^k proxy, which fails to record temperatures higher than 29°C,
28 and Mg/Ca ratios of poorly preserved foraminifera. We reconstruct robust, absolute, SSTs
29 between 13.5 Ma and 9.5 Ma from the South West Indian Ocean (paleolatitude $\sim 5.5^\circ\text{S}$) using
30 Laser-Ablation (LA-) ICP-MS microanalysis of glassy planktic foraminiferal Mg/Ca. Employing
31 this microanalytical technique, and stringent screening criteria, permits the reconstruction of
32 robust paleotemperatures from Mg/Ca thermometry using foraminifera which although glassy,
33 are contaminated by authigenic coatings. Our absolute estimates of 24-31°C suggest that SST in
34 the tropical Indian Ocean was relatively constant between 13.5 and 9.5 Ma, similar to those
35 reconstructed from the tropics using the U_{37}^k alkenone proxy. This suggests an interval of
36 enhanced polar amplification between 10 and 7.5 Ma, immediately prior to the global late
37 Miocene Cooling. The mid-to-late Miocene is proposed as a key interval in the transition of the
38 Earth's climate state towards that of the modern-day.

39

40 1 Introduction

41 The mid-late Miocene is an important interval in the evolution of global climate through
42 the Cenozoic, representing a key period in the transition out of the warm, dynamic climate state
43 of the Miocene Climatic Optimum (MCO) into a more stable unipolar icehouse world (*Badger et al.*,
44 2013; *Foster et al.*, 2012; *Greenop et al.*, 2014; *Sosdian et al.*, 2018). Despite being
45 characterized by similar to modern day atmospheric CO_2 concentrations (*Gavin L. Foster et al.*,
46 2012; *Sosdian et al.*, 2018; *Super et al.*, 2018), middle Miocene mean global temperatures were
47 likely significantly warmer than the modern day (*Pound et al.*, 2011; *Rousselle et al.*, 2013). This
48 has been used to suggest a decoupling of global temperature and atmospheric CO_2 forcing
49 (*LaRiviere et al.*, 2012; *Pagani et al.*, 1999), a characteristic which general circulation models
50 struggle to simulate (*Knorr et al.*, 2011; *von der Heydt and Dijkstra*, 2006). It has also been
51 suggested that the late Miocene was an additional important key step in the transition to our
52 modern climate state, as high latitudes cooled more than low latitudes, leading to a marked
53 steepening of latitudinal temperature gradients (*Herbert et al.*, 2016). The late Miocene Cooling
54 (LMC) between ~ 7.5 and 5.5 Ma was a global phenomenon (*Herbert et al.*, 2016) perhaps
55 associated with decreasing atmospheric $p\text{CO}_2$ (*Stoll et al.*, 2019). The increase in the equator to
56 pole surface temperature gradients was not associated with an increase in the benthic
57 foraminiferal oxygen isotope record, implying that it occurred in the absence of a large increase
58 in continental ice volume (*Herbert et al.*, 2016). Polar amplification in the LMC is consistent
59 with estimates for other time intervals (e.g., *Cramwinckel et al.* (2018)). However, the LMC was
60 also preceded by a significant cooling of mid to high southern and northern latitudes, a
61 heterogenous cooling at high northern latitudes, and a muted, limited cooling in the tropics
62 (*Herbert et al.*, 2016). This perhaps suggests an unusually high polar amplification factor for the
63 interval immediately preceding the LMC. Potential changes in the Earth System that could
64 impact the magnitude of polar amplification include for example sea ice extent, vegetation
65 induced changes in albedo, cloud cover, or ocean-atmosphere heat transport. Constraining the
66 magnitude and timing of the steepening of latitudinal temperature gradients is therefore

67 important for understanding the factors driving the late Miocene surface cooling specifically, and
68 Earth System feedbacks more generally. Ideally, this would be achieved through a combined
69 data-modelling approach using multi-proxy temperature reconstructions spanning a range of
70 latitudes to increase confidence in calculated changes in temperature gradients.
71

72 Despite the significance of this climate interval, the evolution of global sea surface
73 temperatures (SST) and hence temperature gradients during the mid-late Miocene is relatively
74 poorly constrained due to a paucity of complete well-preserved sedimentary successions (*Lunt et*
75 *al.*, 2008). The widespread carbonate dissolution, which dramatically reduced the sediment
76 carbonate content and preservation quality in deep marine sediments, is termed the middle-late
77 Miocene carbonate crash (*Farrell et al.*, 1995; *Jiang et al.*, 2007; *Keller and Barron*, 1987;
78 *Lübbbers et al.*, 2019; *Lyle et al.*, 1995). In addition to these dissolution issues, the majority of
79 foraminifera-bearing Miocene sections are comprised of carbonate rich sediments which have
80 undergone some degree of recrystallisation. The oxygen isotopic composition of planktic
81 foraminifera that have undergone recrystallisation in seafloor sediments has been shown to be
82 biased to colder temperatures (*Pearson et al.*, 2001). While planktic foraminiferal Mg/Ca
83 appears to be less affected than $\delta^{18}\text{O}$, the impact of recrystallisation on reconstructed Mg/Ca sea
84 surface temperatures remains an additional source of uncertainty (*Sexton et al.*, 2006). As a
85 consequence, many mid-late Miocene absolute sea surface temperature reconstructions are
86 restricted to estimates based on the unsaturated alkenone proxy (*Herbert et al.*, 2016; *Huang et*
87 *al.*, 2007; *LaRiviere et al.*, 2012; *Rousselle et al.*, 2013; *Seki et al.*, 2012; *Zhang et al.*, 2014).
88 These records show a cooling in the late Miocene which begins around 10 Ma at high northern
89 and southern latitudes. However, significant cooling in the tropics is not apparent in the alkenone
90 records until ~ 7.5 Ma, while atmospheric $p\text{CO}_2$ reconstructions also suggest a significant decline
91 from this time (*Sosdian et al.*, 2018; *Stoll et al.*, 2019). At face value therefore, these records
92 imply an interval of enhanced polar amplification between 10 Ma and 7.5 Ma in the absence of
93 significant drawdown of CO_2 or increase in ice volume (*Herbert et al.*, 2016; *Sosdian et al.*,
94 2018). One significant caveat to this interpretation is that the Uk_{37} alkenone proxy becomes
95 saturated above 28°C (*Müller et al.*, 1998) and the late Miocene tropical SSTs prior to 7.5 Ma are
96 at this limit (*Herbert et al.*, 2016). Therefore, an alternative interpretation of the data would be
97 that the high latitudes and the tropics cooled synchronously from ~ 10 Ma, but the initial cooling
98 in the tropics was not able to be recorded by the Uk_{37} alkenone proxy. Corroboration of the
99 absolute Uk_{37} alkenone temperatures by an independent proxy would therefore confirm the
100 timing of the global late Miocene Cooling and the possible interval of enhanced polar
101 amplification between 10 Ma and 7.5 Ma.
102

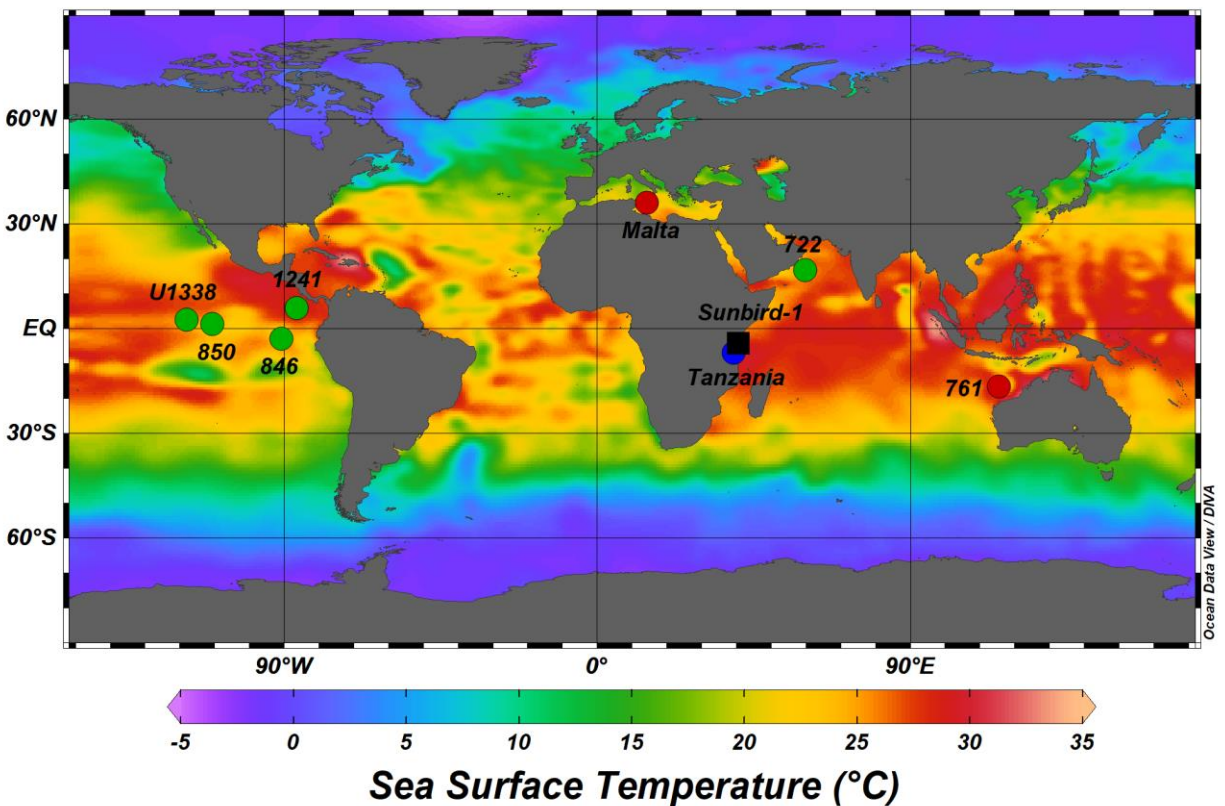
103 Here we present a new planktic foraminiferal Mg/Ca record from the Sunbird-1 industry
104 well cored offshore Kenya by BG Group. Critically, middle to late Miocene sediments in
105 Sunbird-1 are hemipelagic clays, which has resulted in glassy preservation of the foraminifera.
106 However, the foraminifera are coated with metal-rich authigenic coatings, which are not
107 removed by standard cleaning techniques. Planktic foraminifera were therefore analyzed by laser
108 ablation ICP-MS to obtain pristine Mg/Ca of the foraminiferal test carbonate and hence enable
109 estimation of absolute SSTs.
110

111 **2 Materials and Methods**

112 2.1 Site location, stratigraphy, and age control

113 This study utilizes 91 cuttings, spanning 273 meters at burial depths ranging from 630 m
 114 to 903 m, recovered by BG Group from the Sunbird-1 well offshore Kenya (04° 18' 13.268" S,
 115 39° 58' 29.936" E; 723.3 m water depth) (Figure 1, Supplementary Table S1). Sedimentation at
 116 Sunbird-1 through the studied interval (9.5-13.5 Ma) is dominated by clays; the fraction of the
 117 sediment >63 μ m averages 11.5% (Supplementary Table S1), much lower than typical carbonate-
 118 rich deep-water sites. The impermeable nature and chemical composition of clay-rich sediment
 119 reduces diagenetic alteration of primary foraminiferal calcite, making them ideal targets for
 120 geochemical analysis (Pearson *et al.*, 2001; Sexton *et al.*, 2006). Tests displaying the desired
 121 exceptional preservation appear glassy and translucent under reflected light, and SEM imaging
 122 shows retention of the foraminiferal original microstructure (Pearson and Burgess, 2008). This
 123 style of preferential glassy preservation, as displayed in the Sunbird-1 well, is rare to absent in
 124 published records from Miocene foraminifera.

125



126

127

128 **Figure 1:** Location of the Sunbird-1 study site (black square). Other sites for which there are mid
 129 to late Miocene sea surface temperature reconstructions from Mg/Ca (red circles), $\delta^{18}\text{O}$ (blue
 130 circles), and unsaturated alkenones (green circles) are shown. Figure produced using Ocean Data

131 Viewer (*Schlitzer, R., 2018*) using modern-day sea surface temperature data from the World
132 Ocean Database.

133

134 Micropaleontological and calcareous nannoplankton assemblages for Sunbird-1 were
135 analyzed by Haydon Bailey and Liam Gallagher of Network Stratigraphic Consulting.
136 Biostratigraphic datums, correlated with the astronomical timescale of *Gradstein et al. (2004)*,
137 are based on the planktic foraminifera zonations of *Wade et al. (2011)* and calcareous nanofossil
138 zonations of *Backman et al. (2012)*. An age model was constructed by linear interpolation
139 between these biostratigraphic datums (Figure S1). Sedimentation rates were ~3 cm/kyr
140 immediately following the middle Miocene Climate Transition (MMCT), and subsequently
141 increased to ~17 cm/kyr between 11.8 and 11.5 Ma, before decreasing to ~8 cm/kyr until 9.5 Ma.

142

143 2.2 Foraminiferal stable isotope analysis

144 Up to 12 individual tests of the planktic foraminifer *Globigerinoides obliquus* showing
145 glassy preservation were used. *G. obliquus* is an extinct, symbiont bearing species with a tropical
146 to subtropical paleogeographical distribution, and is interpreted as being a surface mixed-layer
147 dweller (*Aze et al., 2011; Keller, 1985*). The assertion that *G. obliquus* inhabits and calcifies in
148 the surface mixed layer (*Aze et al., 2011; Keller, 1985*) is supported by multispecies analyses
149 from a 10.0 Ma sediment sample from the Indian Ocean offshore Tanzania showing *G. obliquus*
150 to have the most negative $\delta^{18}\text{O}$ (-2.5‰) of all species (Paul Pearson, personal communication,
151 2019). Tests were crushed between two glass plates ensuring all chambers were opened. Any
152 visible infill was removed using a fine paintbrush under a binocular microscope. Fine clays and
153 other detrital material on the outer surface of the test were removed by rinsing three times in 18.2
154 M Ω DI water, ultrasonicing for 5-10 seconds in analytical grade methanol, and finally rinsing a
155 further time in 18.2 M Ω DI water. Samples were analyzed at Cardiff University on a
156 ThermoFinnigan MAT253 with online sample preparation using an automated Kiel IV carbonate
157 device. Results are reported relative to Pee Dee Belemnite, and long-term uncertainty based on
158 repeat analysis of NBS-19 is ± 0.08 ‰ (n=469, 2 standard deviations) and on repeat analysis of
159 BCT63 is ± 0.07 ‰ (n=310, 2 standard deviations). Data is available in Supplementary Table S2.

160

161 2.3 Solution ICP-MS trace metal analysis

162 Between 10 and 15 individuals of the planktic foraminifer *Dentoglobigerina. altispira*
163 were crushed between two glass plates ensuring all chambers were opened. Due to the low
164 foraminiferal abundance it was not possible to analyze the same species for stable isotope and
165 trace metal composition. Any visible infill was removed using a fine paintbrush under a
166 binocular microscope. Fragments were cleaned to remove clays and organic matter following the
167 standard protocol (*Barker et al., 2003; Boyle and Keigwin, 1985*). Due to the clay rich nature of
168 the sediment the clay removal procedure was conducted twice. To test for the possible presence
169 of metal oxides half of the samples were reductively cleaned between the clay removal and
170 oxidative cleaning steps. Samples were dissolved in trace metal pure 0.065 M HNO₃ and diluted
171 with trace metal pure 0.5M HNO₃ to a final volume of 350 μl . Samples were analyzed at Cardiff
172 University on a Thermo Element XR ICP-MS using standards with matched calcium

173 concentrations to reduce matrix effects (*Lear et al.*, 2010; *Lear et al.*, 2002). Together with
174 Mg/Ca, several other ratios (Al/Ca, Mn/Ca, and U/Ca) were analyzed to screen for potential
175 contaminant phases. Data are available in Supplementary Table S3. Long-term analytical
176 precision for Mg/Ca throughout the study is better than 2%.
177

178 2.4 Laser ablation-ICP-MS analysis

179 Direct sampling of solid phase material via laser ablation (LA-) allows for geochemical
180 analyses through individual foraminiferal tests at the sub-micron scale when coupled to an
181 inductively-coupled-plasma mass spectrometer (ICP-MS) (*Detlef et al.*, 2019; *Eggins et al.*,
182 2004; *Evans et al.*, 2015; *Fehrenbacher et al.*, 2015; *Hines et al.*, 2017; *Petersen et al.*, 2018;
183 *Reichart et al.*, 2003). A key advantage of analyzing the trace element composition of
184 foraminifera using LA-ICP-MS over the more traditional solution based ICP-MS is the ability to
185 recognize the diagenetically altered portions of the tests, allowing identification of the primary
186 calcite (*Creech et al.*, 2010; *Hasenfratz et al.*, 2016; *Pena et al.*, 2005). The elemental
187 composition of this primary calcite can provide uncompromised information about
188 palaeotemperature (*Nooijer et al.*, 2017; *Eggins et al.*, 2003; *Pena et al.*, 2005) and other paleo-
189 environmental conditions such as pH (*Mayk et al.*, 2020; *Thil et al.*, 2016) and oxygenation
190 (*Koho et al.*, 2015; *Petersen et al.*, 2018).
191

192 Up to six specimens of *D. altispira* were selected from 44 depth intervals through the
193 Sunbird-1 core for LA-ICP-MS analysis. Foraminiferal sample preparation included the removal
194 of fine clays and other detrital material on the outer surface of the test using DI water and
195 methanol, but the more aggressive oxidative and reductive steps (*Barker et al.*, 2003; *Boyle and*
196 *Keigwin*, 1985), were not required for laser ablation analysis (*Vetter et al.*, 2013). The cleaned
197 tests were mounted onto glass slides using double sided carbon tape and were allowed to dry
198 before being mounted into the sample cell (*Evans et al.*, 2015; *Fehrenbacher et al.*, 2015; *Hines*
199 *et al.*, 2017).
200

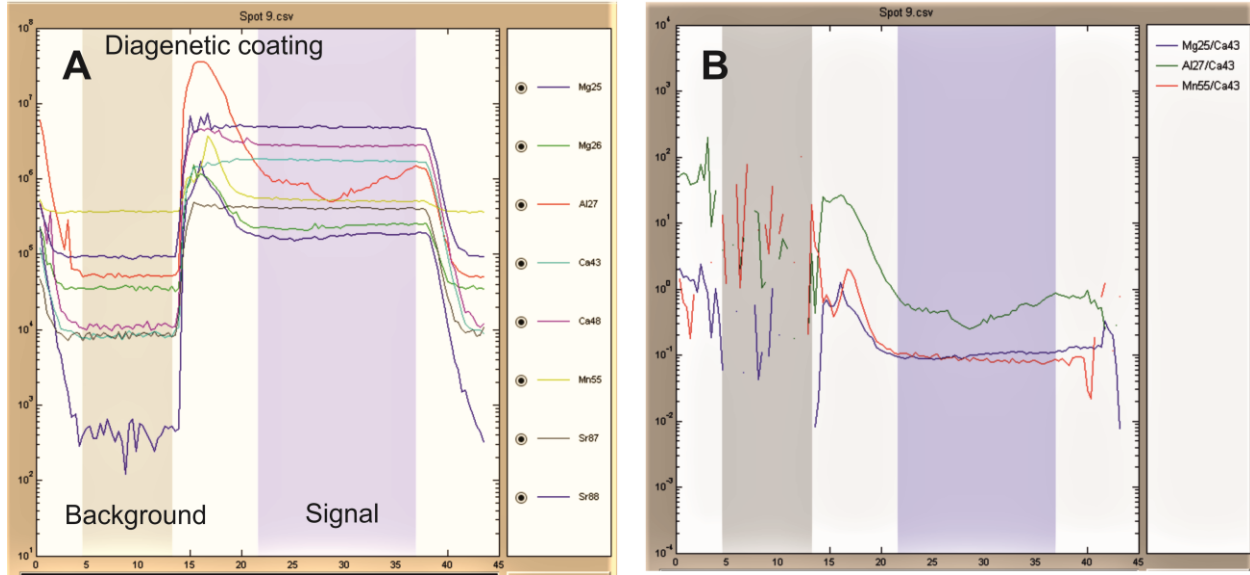
201 Analyses were performed using an ArF excimer (193nm) LA- system with dual-volume
202 laser-ablation cell (RESOLUTION S-155, Australian Scientific Instruments) coupled to a Thermo
203 Element XR ICP-MS. Optimized ablation parameters and analytical settings determined for
204 analyzing foraminifera in the Cardiff University CELTIC laboratory (Supplementary Table S4;
205 (*Detlef et al.*, 2019; *Nairn*, 2018)) were used for this study. Three cleaning pulses to remove any
206 contaminant on the outer ~0.5 μm of the test surface were included prior to analysis. We
207 analyzed ^{25}Mg , ^{27}Al , ^{43}Ca , ^{55}Mn and ^{88}Sr , each isotope having a constant 50 ms dwell time.
208 Typically, intervals with elevated Mn and Al in concert with elevated Mg are interpreted as
209 being contaminant phases (e.g., Fe-Mn oxides-hydroxides or clays), and are commonly found on
210 the inner and outer test surface (*Barker et al.*, 2003; *de Nooijer et al.*, 2014; *Hasenfratz et al.*,
211 2016; *Koho et al.*, 2015; *Pena et al.*, 2005).
212

213 Where possible three laser spot depth profiles, each approximately 15 μm deep assuming
214 that each laser pulse only ablates a very thin, ~0.1 μm , layer of calcite, were collected on each of
215 the penultimate (f-1) and previous (f-2) chambers. However, this was not always possible such

216 that older chambers were frequently used to ensure six laser spots per specimen were analyzed
217 (*Nairn, 2018*). NIST SRM 610 glass standard was measured between every six laser profiles, and
218 NIST SRM 612 at the beginning and end of analyses from each sample depth. The reference
219 values for elemental concentrations in both silicate glass standards are taken from the GEOREM
220 website (http://georem.mpch-mainz.gwdg.de/sample_query_pref.asp), updated from *Jochum et*
221 *al.* (2011). NIST SRM 612 was used to determine long term external reproducibility using NIST
222 SRM 610. For Mg/Ca NIST 612 (n=90) had an accuracy of 12.0% and a precision of 3.7%
223 relative to the reported value. A similar ~12% negative offset relative to the reported value of
224 NIST 610-calibrated NIST 612 has been observed over a much longer period of data collection
225 (*Evans and Müller, 2018*). The NIST 610-calibrated data presented here supports the
226 determination of *Evans and Müller* (2018) that the Mg values for both NIST 610 and NIST 612
227 require reassessment. A more thorough assessment of accuracy cannot be made at present, as a
228 well-characterized calcite reference material, matrix matched to typical foraminiferal calcite, is
229 not currently available (*Evans et al., 2015; Evans and Müller, 2018; Fehrenbacher et al., 2015*).
230

231 2.5 LA-ICP-MS data processing and screening

232 Each individual laser ablation profile was carefully inspected and processed using the SILLS
233 data reduction software package (*Guillong et al., 2008*) following the established protocol
234 outlined in *Longerich et al.* (1996). First, a background signal of ~15 seconds, from data
235 acquired when the laser was turned off prior to ablation, was selected for each profile. Following
236 this the integration interval for the profile was selected based upon the following three criteria:
237 (i) stable ^{43}Ca counts, indicating ablation of calcite, (ii) stable Mg/Ca signal, indicating a
238 consistent primary calcite phase, (iii) flat Mn/Ca and Al/Ca signals, avoiding any peaks
239 indicating intervals of contamination (Figure 2).
240



241

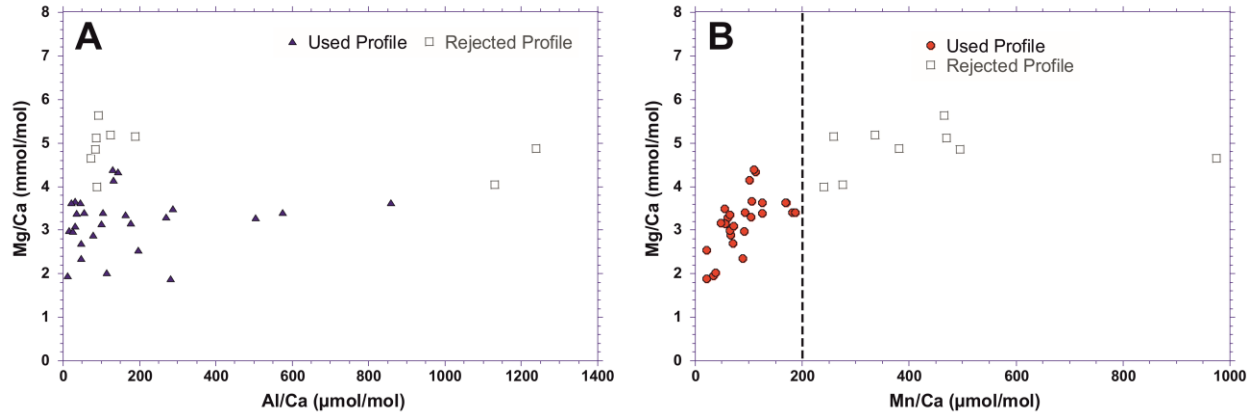
242 **Figure 2:** Representative LA-ICP-MS Mg, Al, and Mn profiles demonstrating the selection of
 243 background (grey panel) and sample (blue panel) signals, shown in raw isotopic counts (A), and
 244 ratios mode (B) where the isotopes of interest are relative to ^{43}Ca , the internal standard. In both
 245 panels the x axis is analysis time (seconds), and the y axis is the raw intensity of the isotopes (A)
 246 or ratios (B) on a log scale. The sample interval is selected to avoid the elevated Mg/Ca, Mn/Ca,
 247 and Al/Ca at the outer surface of the test.

248

249

250 Individual depth profiles were corrected by first subtracting the mean background signal. The
 251 repeated analysis of the NIST 610 standard reference material was used to linearly correct for
 252 any instrumental drift. Typically, this is small, <2%, because of the good counting statistics and
 253 stable data acquisition during ablation. The ablation profiles were normalized to ^{43}Ca as the
 254 internal standard and elemental concentrations (TM/Ca) were calculated, assuming 40 wt % for
 255 CaCO_3 . Integrated depth profiles which display $\text{Mn/Ca} > 200 \mu\text{mol/mol}$ were excluded, as these
 256 suggest potential contamination by Mn-oxides. Furthermore, integrated depth profiles with Al/Ca
 257 $> 100 \mu\text{mol/mol}$ associated with elevated Mg/Ca were also excluded (e.g. Figure 3).

258



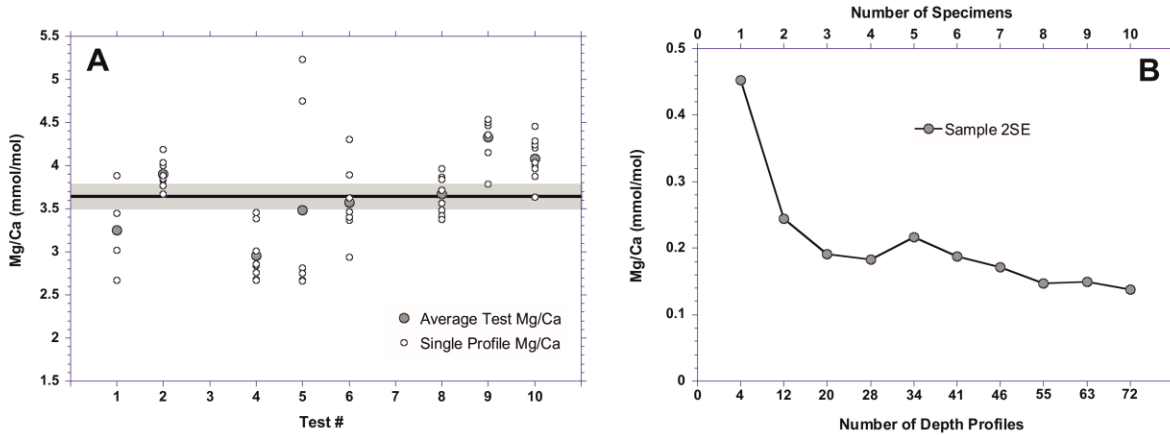
259

260 **Figure 3:** Covariance between *D. altispira* Mg/Ca and (a) Al/Ca, and (b) Mn/Ca from LA-ICP-
 261 MS profiles from the 1539-1542 m sample. Used profiles are filled blue triangles and red circles,
 262 respectively, whereas profiles excluded during screening are open squares.
 263

264 2.6 Determination of mean foraminiferal test Mg/Ca by laser ablation

265 Geochemical heterogeneity exists both within an individual foraminiferal test and
 266 between foraminiferal tests from the same sample (*Eggins et al., 2004; Fehrenbacher and*
 267 *Martin, 2014; Sadekov et al., 2008; Sadekov et al., 2005*). Therefore, several laser ablation
 268 profiles are required to produce a consistent Mg/Ca ratio for temperature reconstructions. Here
 269 we analyzed ten depth profiles through each of ten individual *D. altispira* tests from the 1551-
 270 1554 m (11.74 Ma) sample to determine representative inter-specimen variability for these
 271 samples (Figure 4). Approximately one third ($n=28$) of the 100 depth profiles were excluded
 272 during screening for elevated Al/Ca and Mn/Ca indicative of diagenetic contamination. The
 273 Mg/Ca value of individual depth profiles in *D. altispira* from the 1551-1554 m sample ranges
 274 from 2.67 mmol/mol to 5.23 mmol/mol, with a mean of 3.63 ± 0.14 mmol/mol ($n=72$) (Figure
 275 4a; Supplementary Table S5). The mean Mg/Ca value from four specimens, a total of 28 profiles,
 276 is 3.41 ± 0.18 mmol/mol (Figure 4a). Averaging profiles from ten individual tests did therefore
 277 not produce significantly better accuracy or precision than averaging profiles from four
 278 individual tests (Figure 4b). Therefore, for a Mg/Ca ratio to be considered representative it must
 279 represent an average of at least 28 laser ablation profiles, from at least four specimens, with the
 280 analytical uncertainty (2 SE) indicating the intra- and inter-specimen variability this incorporates.
 281 To account for depth profiles excluded due to contamination, where possible the number of
 282 measurements per sample was increased to 36, six depth profiles per specimen and six specimens
 283 per sample. This result is in line with other LA-ICP-MS studies (*Rathmann et al., 2004; Sadekov*
 284 *et al., 2008*). Future studies are advised to conduct similar testing to determine the number of
 285 measurements required for a mean sample Mg/Ca to be representative, as this will likely be site
 286 dependent.

287



288

289 **Figure 4:** Distribution of *D. altispira* Mg/Ca values from LA-ICP-MS profiles of the 1551-1554
 290 m sample. (A) A summary of all Mg/Ca values, where open circles denote individual
 291 measurements, and filled circles denote mean Mg/Ca values for each specimen. The horizontal
 292 black line is the mean of all depth profiles from the sample, and the grey bar the ± 2 SE sample
 293 uncertainty. (B) The evolution of the sample 2 SE with increasing specimens. Only profiles that
 294 passed data screening are included (n=72). Data is from Supplementary Table S5.
 295

296

2.7 Mg/Ca paleo-sea surface temperature calculations

297

298

299

300

301

302

303

304

305

306

307

308

309

310

311

312

313

314

315

316

317

Planktic foraminiferal Mg/Ca is influenced by changes in the carbonate system, the ratio increasing with decreased pH and/or $\Delta[\text{CO}_3^{2-}]$ (Evans *et al.*, 2016; Gray and Evans, 2019; Gray *et al.*, 2018; Russell *et al.*, 2004; Yu and Elderfield, 2008). However, the ultimate driver of this effect is not certain, and it has been shown that for *Orbulina universa* DIC plays a role in test Mg/Ca variability (Holland *et al.*, 2020). We follow recent results which interpret pH, as opposed to $\Delta[\text{CO}_3^{2-}]$ or DIC, as the parameter which controls the carbonate system's influence on Mg/Ca (Evans *et al.*, 2016; Gray *et al.*, 2018). Furthermore, unlike with $\Delta[\text{CO}_3^{2-}]$, it is possible to reconstruct pH through the Neogene using boron isotopes in foraminifera (Foster and Rae, 2015; Greenop *et al.*, 2014; Hennehan *et al.*, 2013; Sosdian *et al.*, 2018). Here we use the recent Neogene boron isotope compilation of Sosdian *et al.* (2018), which provides well constrained estimates of pH across this time interval (Figure S2). Linear interpolation between these pH values allows us to estimate a mean pH value, and associated uncertainty envelope, for each Sunbird-1 sample, where the uncertainty envelope is maximum and minimum pH at the 17% and 83% confidence interval ($\sim \pm 0.06$ pH units). Measured planktic foraminiferal Mg/Ca

318 values are corrected for this influence of pH using the equation of *Evans et al.* (2016) (Equation
 319 1).
 320

$$\text{Equation 1: } \text{Mg/Ca}_{\text{CORRECTED}} = \frac{\text{Mg/Ca}_{\text{MEASURED}}}{\frac{0.66}{1 + \exp(6.9(\text{pH} - 8.0))} + 0.76}$$

321

322 Fluxes of Mg^{2+} and Ca^{2+} into and out of the oceans means seawater Mg/Ca (Mg/Ca_{sw})
 323 experiences secular variation. This variability must be accounted for when determining absolute
 324 sea surface temperatures on Cenozoic timescales (*Hollis et al.*, 2019). Reconstructions of
 325 Mg/Ca_{sw} based on large benthic foraminifera (*Evans et al.*, 2018), calcite veins (*Coggon et al.*,
 326 2010), fluid inclusions (*Horita et al.*, 2002), and echinoderms (*Dickson*, 2002) have constrained
 327 this variability through the Cenozoic (Figure S3). The Eocene-Oligocene demonstrates relatively
 328 stable values of 2.0-2.5 mol/mol (*Coggon et al.*, 2010; *Evans et al.*, 2018). However, only one
 329 data point exists from the Miocene, through which Mg/Ca_{sw} more than doubles from ~2.2
 330 mol/mol in the late Oligocene (*Coggon et al.*, 2010) to the well constrained value of 5.2 mol/mol
 331 in the modern ocean (*Broecker et al.*, 1982; *Dickson*, 2002; *Horita et al.*, 2002; *Kısakürek et al.*,
 332 2008). Therefore, the method of *Lear et al.* (2015) is followed by fitting the fourth-order
 333 polynomial curve fit through the compiled seawater Mg/Ca (Mg/Ca_{sw}) proxy records (Figure
 334 S3). We use a ± 0.5 mol/mol uncertainty window in the following temperature calculations, this
 335 error envelope incorporating the majority of the spread in the proxy data (Figure S3). The
 336 preferred equation of (*Evans et al.*, 2016) is used to account for the influence of changing
 337 Mg/Ca_{sw} when estimating SST. These authors determined that the best fit to culture-derived
 338 calibration lines is when both the pre-exponential (B) and exponential (A) coefficients vary
 339 quadratically with Mg/Ca_{sw} (Equation 2 and 3).
 340

341 **Equation 2: $B = (0.019 \times \text{Mg/Ca}_{\text{sw}}^2) - (0.16 \times \text{Mg/Ca}_{\text{sw}}) + 0.804$**

342 **Equation 3: $A = (-0.0029 \times \text{Mg/Ca}_{\text{sw}}^2) + (0.032 \times \text{Mg/Ca}_{\text{sw}})$**

343 We substitute these equations into the general exponential calibration, $\text{Mg/Ca} = B \exp^{AT}$,
 344 to account for changing Mg/Ca_{sw} . Although the *Evans et al.* (2016b) equation is specific to
 345 *Globigerinoides ruber*, this species inhabits a shallow water depth of 0-50m (*Schiebel and*
 346 *Hemleben*, 2017) similar to the inferred mixed-layer habitat depth *D. altispira* (*Aze et al.*, 2011).
 347 Furthermore, as with *G. ruber*, *D. altispira* was a tropical/subtropical species, with symbionts
 348 (*Aze et al.*, 2011).
 349

350 Salinity can exert a secondary effect on foraminiferal Mg/Ca, sensitivity measurements
 351 from culture and core-top studies show this to be ~3-5% per practical salinity unit (psu) (*Gray et*
 352 *al.*, 2018; *Hollis et al.*, 2019; *Hönisch et al.*, 2013; *Kısakürek et al.*, 2008). In the absence of a
 353 robust, independent salinity proxy (although we do note the promise of Na/Ca (*Bertlich et al.*,

2018; Geerken *et al.*, 2018)) and the relatively minor effect of salinity on foraminiferal Mg/Ca, this potential secondary control is not empirically accounted for. Sunbird-1 was located in a coastal setting and likely experienced a highly variable hydrological cycle due to changes in the position of the ITCZ making it susceptible to changes in salinity. Therefore, an error of $\pm 0.5^\circ\text{C}$ is incorporated into the final sea surface temperature estimates, equivalent to an assumed salinity variability of $\sim\pm 1$ PSU.

The uncertainties ($\pm 2\text{SE}$) associated with the conversion from Mg/Ca to absolute SST estimates incorporates the uncertainty in the pH correction, the uncertainty on the $\text{Mg}/\text{Ca}_{\text{sw}}$ record, and a potential uncertainty due to varying salinity. This is termed the calibration uncertainty and is considerably greater than the independent analytical uncertainty.

2.8 $\delta^{18}\text{O}$ paleo-sea surface temperature calculations

Due to the limited sampling resolution of the trace metal data, SST is also calculated using foraminiferal $\delta^{18}\text{O}$. Foraminiferal $\delta^{18}\text{O}$ ($\delta^{18}\text{O}_{\text{calcite}}$) is converted to temperature (T) using the palaeotemperature equation of Bemis *et al.* (1998) (Equation 4), changes in global ice volume being corrected using the $\delta^{18}\text{O}_{\text{sw}}$ value from the nearest 0.1 Myr time interval in the compilation of Cramer *et al.* (2011).

$$\text{Equation 4: } (\delta^{18}\text{O}_{\text{calcite}} - \delta^{18}\text{O}_{\text{sw}} + 0.27) = -0.21 \pm 0.003 T + 3.10 \pm 0.07$$

The absence of a robust, independent salinity proxy makes any quantitative attribution of its influence on foraminiferal $\delta^{18}\text{O}$ challenging. Therefore, we incorporate potential $\delta^{18}\text{O}$ variability due to salinity into any temperature estimate uncertainty. Salinity of the upper water column in a $0.75^\circ \times 0.75^\circ$ grid square around the modern-day study site varies between 34.9 and 35.4 PSU (Boyer *et al.*, 2013). Using the Indian Ocean $\delta^{18}\text{O}_{\text{sw}}$ -salinity relationship of LeGrande and Schmidt (2006) (Equation 5) this equates to a maximum $\delta^{18}\text{O}_{\text{sw}}$ uncertainty of $\pm 0.091\text{‰}$. Using Equation 4 this equates to a 0.4°C uncertainty in the calculated surface temperature.

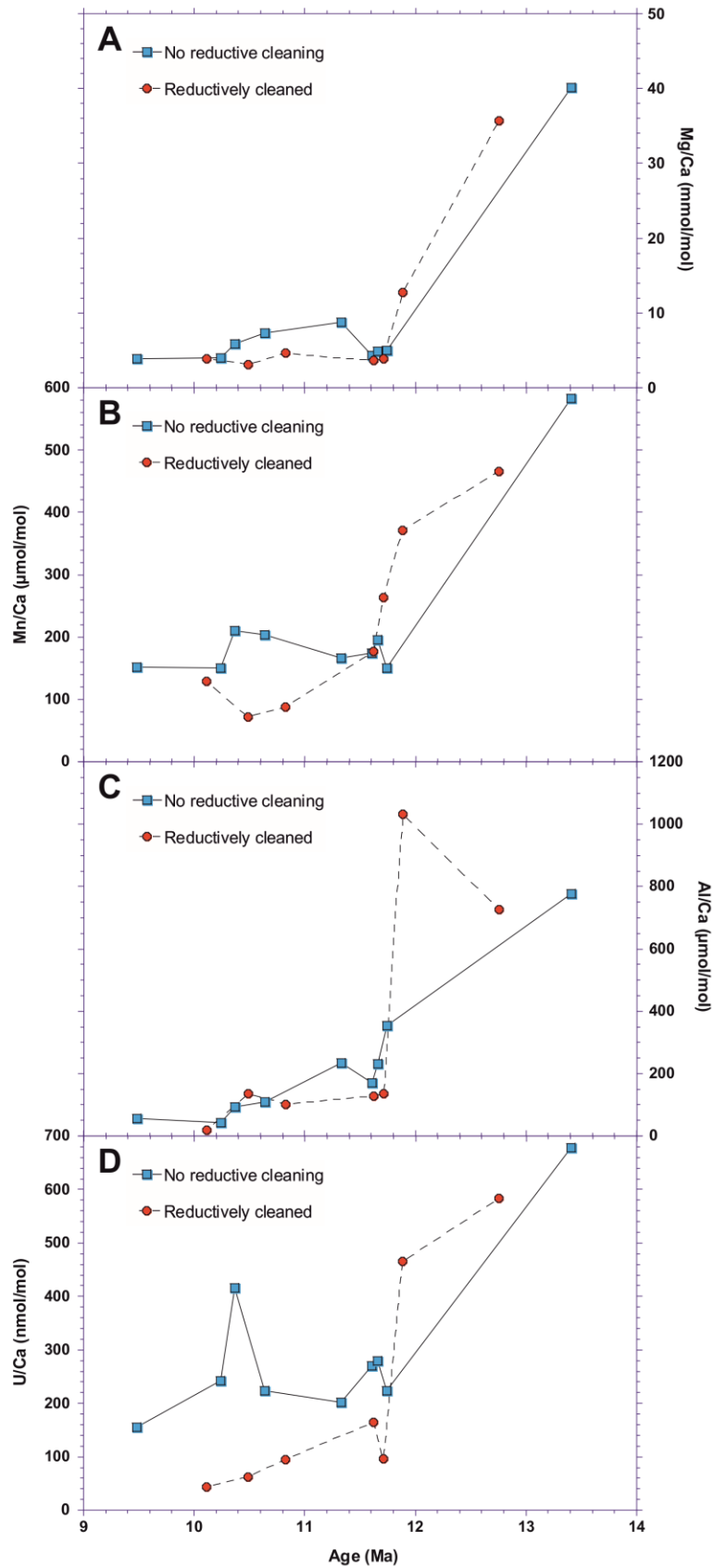
$$\text{Equation 5: } \delta^{18}\text{O}_{\text{sw}}(\text{SMOW}) = (0.16 \pm 0.004 \times \text{Salinity}) - 5.31 \pm 0.135$$

We acknowledge the likelihood of increased variability in sea surface salinity in this downcore record, more than the modern-day calibration accounts for. We use the paleolatitude calculator of van Hinsbergen *et al.* (2015) to calculate a paleolatitude for Sunbird-1 at 10 Ma of approximately 5.5°S . Using the latitudinal correction of Zachos *et al.* (1994), this gives a $\delta^{18}\text{O}_{\text{sw}}$ of 0.1‰ . The absence of a significant offset from ‰SMOW (0‰) suggests that this will have a negligible influence on the isotopic SST reconstructions.

390 **3 Results**

391 3.1 Solution ICP-MS trace element chemistry

392 *D. altispira* Mg/Ca measured by solution ICP-MS ranges from 3.15 ± 0.1 to 40.2 ± 0.2
393 mmol/mol (Figure 5a), translating to unrealistically high reconstructed sea surface temperatures.
394 The high Mg/Ca ratios strongly suggest the addition of magnesium from a secondary, post-
395 depositional source, prior to 11.75 Ma. The elevated Mg/Ca ratios are associated with
396 correspondingly high Mn/Ca, Al/Ca, and U/Ca (Figure 5b-d). All but two of the Mn/Ca ratios are
397 in excess of the proposed 100 $\mu\text{mol/mol}$ threshold above which its role as a potential
398 contaminant must be assessed (Boyle, 1983). Furthermore, every foraminiferal U/Ca ratio is
399 considerably higher than typical U/Ca ratios of primary foraminiferal calcite, which range from
400 $\sim 3\text{-}23$ nmol/mol (Chen *et al.*, 2017; Raitzsch *et al.*, 2011; Russell *et al.*, 2004). In addition,
401 foraminiferal Al/Ca exceeds the commonly applied 100 $\mu\text{mol/mol}$ threshold in all but the four
402 youngest samples.
403



405 **Figure 5:** Downcore (a) Mg/Ca, (b) Mn/Ca, (c) U/Ca, and (d) Al/Ca records for *D. altispira* in
406 the Sunbird-1 core, distinguishing between sample that were reductively cleaned (red circles)
407 and those that were not (blue squares).
408

409 The presence of elevated foraminiferal Mn/Ca, Al/Ca, and U/Ca ratios does not
410 necessarily mean that the Mg/Ca ratios are contaminated. However, the downcore, point to point
411 correlation (Figure 5) and covariance (Supplementary Figure S4) between Mg/Ca and
412 contaminant indicators suggest a strong association. This downcore association between Mg/Ca
413 and contaminant indicators, despite a rigorous chemical cleaning protocol, suggests one of two
414 things; (i) the chemical cleaning protocol is not fully effective at removing contaminant coatings,
415 and/or (ii) an Mg-rich contaminant phase is pervasive throughout the calcite test.
416

417 Including the reductive cleaning step lowers Mg/Ca, Mn/Ca, and U/Ca ratios in the post
418 11.8 Ma portion of the record, but has a negligible effect on Al/Ca. Neither cleaning protocol is
419 effective at removing the authigenic coatings on the Sunbird-1 foraminifera in the pre 11.8 Ma
420 portion of the record (Figure 5). For this reason, we also analyzed Sunbird-1 planktic
421 foraminifera by laser ablation ICP-MS.
422

423 3.3 Downcore Laser Ablation ICP-MS Mg/Ca

424 Our laser ablation profiles clearly demonstrate that the metal-rich contaminant is present
425 as an authigenic surface coating on the glassy foraminifera (e.g., Figure 2). Because the
426 alteration is not pervasive throughout the calcite test, laser ablation ICP-MS is an ideal approach
427 to determine pristine test Mg/Ca on these coated samples (section 2.6). *D. altispira* Mg/Ca
428 determined by laser-ablation ICP-MS ranges from 3.03 to 5.07 mmol/mol, with an average value
429 of 4.18 ± 0.40 mmol/mol, and errors ($\pm 2SE$) range from 0.10 to 1.04 mmol/mol (Supplementary
430 Table S6). However, due to elevated Al/Ca and Mn/Ca ratios, only 14 of the 44 samples are
431 represented by at least 28 laser profiles. To alleviate this problem, adjacent samples have been
432 combined into longer time slices to ensure that the absolute mean Mg/Ca measurements are
433 robust (Table 1). Samples comprising the mean of at least 28 laser profiles are termed “un-
434 pooled samples”. Samples pooled to achieve a minimum of 28 laser profiles are termed “pooled
435 samples”. It is acknowledged that by combining adjacent samples, which span up to 420 kyr,
436 could incorporate orbital scale climatic variability into these pooled samples. However, we do
437 not infer climatic variability on orbital timescales because the coarse sampling resolution could
438 incorporate aliasing of any precessional or obliquital periodicity into longer term eccentricity
439 cycles (*Pisias and Mix*, 1988). In fact, by combining adjacent samples to generate a
440 representative mean Mg/Ca for a longer time-slice could in fact smooth orbital scale variability,
441 reducing uncertainty and assisting the interpretation of longer-term climatic trends.
442

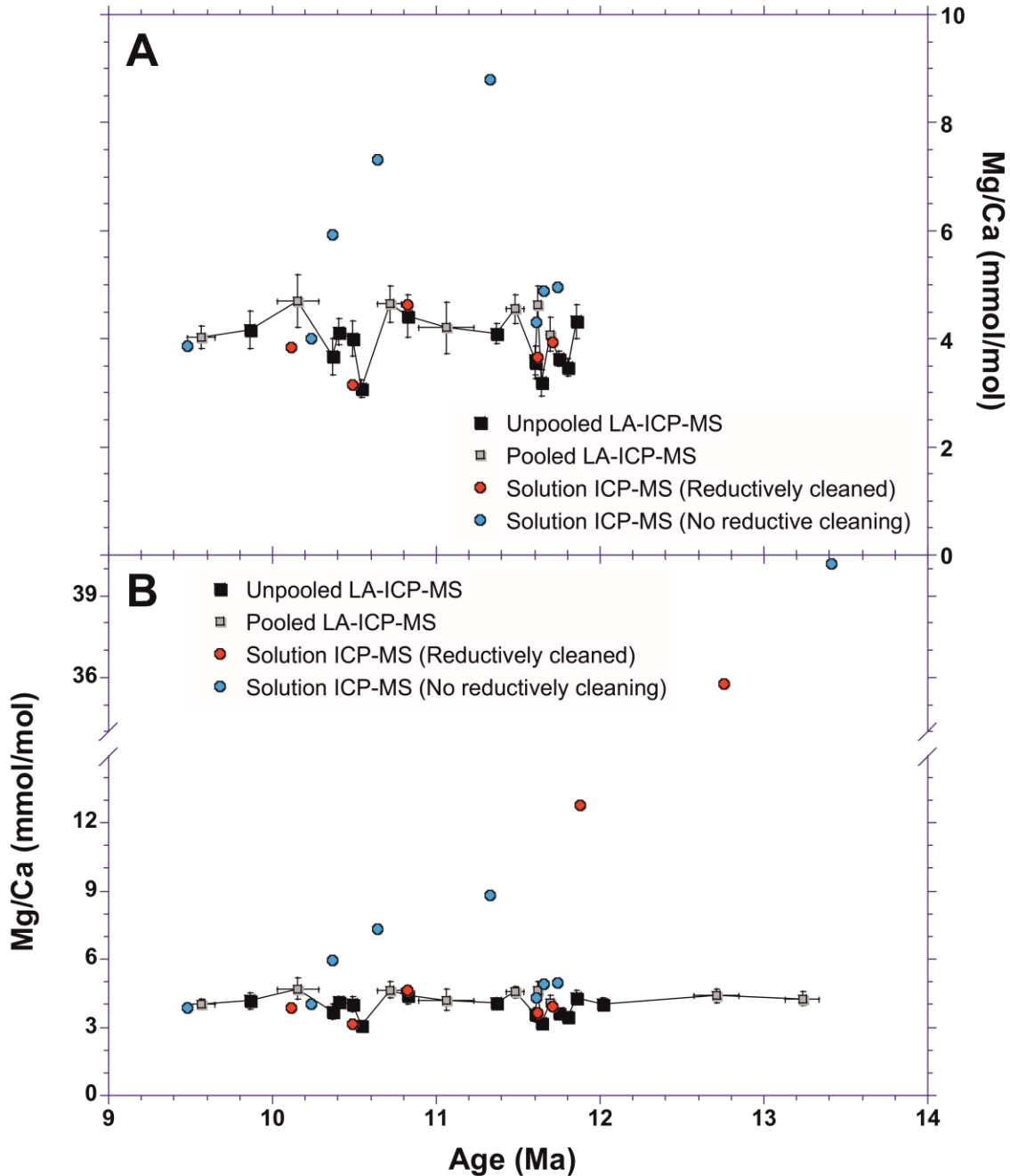
443

444

Average Age (Ma)	Minimum Age (Ma)	Maximum Age (Ma)	# Samples Pooled	# Specimens Used	# Profiles used	Sample Mean Mg/Ca (mmol/mol)	Sample 2 SE
9.57	9.48	9.65	3	13	51	4.02	0.21
10.15	10.03	10.28	2	8	24	4.70	0.48
10.72	10.64	10.79	2	9	39	4.65	0.34
11.06	10.89	11.23	5	11	22	4.20	0.48
11.48	11.43	11.53	3	13	40	4.55	0.26
11.70	11.67	11.72	2	9	35	4.09	0.31
12.71	12.57	12.85	4	12	50	4.40	0.31
13.24	13.13	13.34	3	7	25	4.26	0.31

445 **Table 1:** Age range and the number of samples, specimens, and profiles combined for each
 446 pooled sample of *D. altispira* from Sunbird-1.
 447

448 The mean Mg/Ca of representative samples after incorporating the nine pooled Mg/Ca
 449 samples with the 14 un-pooled samples ranges from 3.08 to 4.70 mmol/mol, with an average
 450 value of 4.04 ± 0.29 mmol/mol, and errors ($\pm 2SE$) range from 0.14 to 0.48 mmol/mol
 451 (Supplementary Table S7). These values are in good agreement with the reductively cleaned
 452 solution ICP-MS data for the post-11.8 Ma portion of the record (Figure 6a). However, we can
 453 be more confident that the laser ablation data are not biased by authigenic coatings, and the laser-
 454 ablation approach has the advantage that we can also determine original test Mg/Ca in the older
 455 part of the record (Figure 6b).
 456



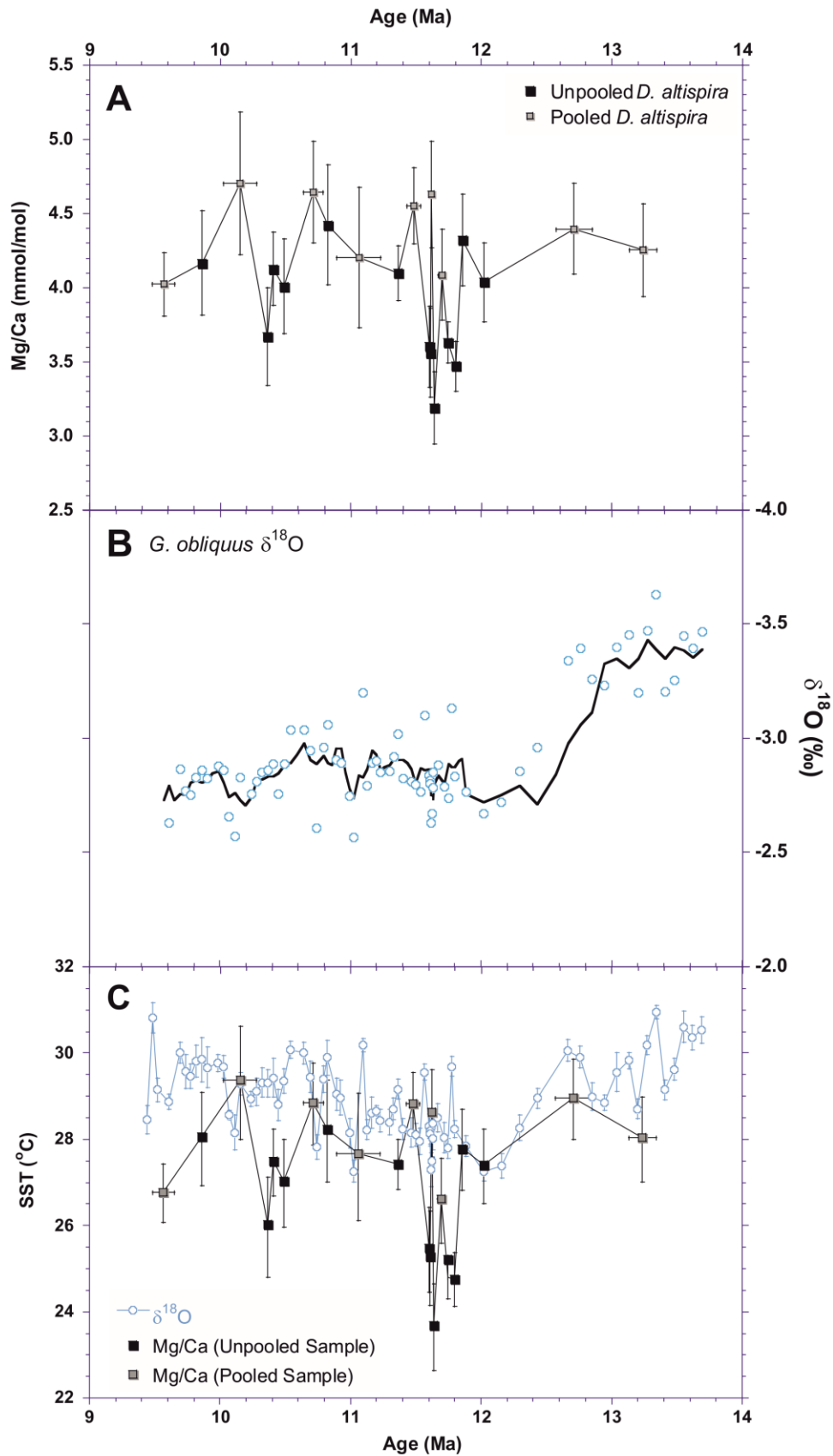
457

458 **Figure 6:** Comparison of solution based (red circles with reductive cleaning, and blue circles
 459 without reductive cleaning) and LA-ICP-MS (black squares denoting unpooled samples, and
 460 grey squares denoting pooled samples) *D. altispira* Mg/Ca at Sunbird-1 from the intervals (a)
 461 after 11.8 Ma, and (b) the full record. Error bars on the LA-ICP-MS data denote the age range
 462 for pooled samples and the ± 2 SE of Mg/Ca from all depth profiles in the sample. Note the break
 463 between 13 mmol/mol and 35 mmol/mol in (b).
 464

465 There is no obvious long-term trend in Mg/Ca through the interval (Figure 7a). Between
466 11.8 Ma and 11.7 Ma there is a 0.7-0.8 mmol/mol decrease in Mg/Ca followed by a recovery to
467 approximately previous values at 11.5-11.4 Ma. There is a Mg/Ca decrease of similar magnitude
468 from between 10.7 Ma and 10.36 Ma, recovering by 9.85 Ma. We acknowledge that the coarse
469 sampling frequency, and the combining of samples could be obscuring similar variability
470 through the rest of the record.
471

472 3.4 *G. obliquus* $\delta^{18}\text{O}$

473 *G. obliquus* $\delta^{18}\text{O}$ ranges from -3.63‰ to -2.34‰ with a mean value of -2.92‰. The $\delta^{18}\text{O}$
474 record shows very little variability, values remaining stable at -3.4‰ prior to a positive 0.6‰
475 shift at ~12.5 Ma, and -2.7‰ after (Figure 7b). This translates to a stable $\delta^{18}\text{O}$ SST record,
476 temperatures ranging between 27°C and 31°C with the only distinctive trend being a ~3°C
477 decrease between ~12.7 Ma and 12.0 Ma.
478



480 **Figure 7:** (a) Mean *D. altispira* LA-ICP-MS Mg/Ca ratios (mmol/mol) for unpooled (black
 481 squares) and pooled (grey squares) samples from Sunbird-1. Error bars denote the age range for
 482 pooled samples, and the $\pm 2\text{SE}$ of Mg/Ca from all depth profiles in the sample. (b) *G. obliquus*
 483 $\delta^{18}\text{O}$ from Sunbird-1. Solid line is a five-point moving average. (c) Sea surface temperature
 484 records at Sunbird-1 from planktic foraminiferal $\delta^{18}\text{O}$ and LA-ICP-MS Mg/Ca. Symbols are the
 485 same as in (a) and (b). Error bars on the $\delta^{18}\text{O}$ record denote the analytical uncertainty ($\pm 2\text{SD}$),
 486 and error bars on the Mg/Ca record denote the sample uncertainty ($\pm 2\text{SE}$). As in (a), pooled
 487 Mg/Ca samples also have horizontal error bars denoting the age range the sample incorporates.
 488

489 4 Discussion

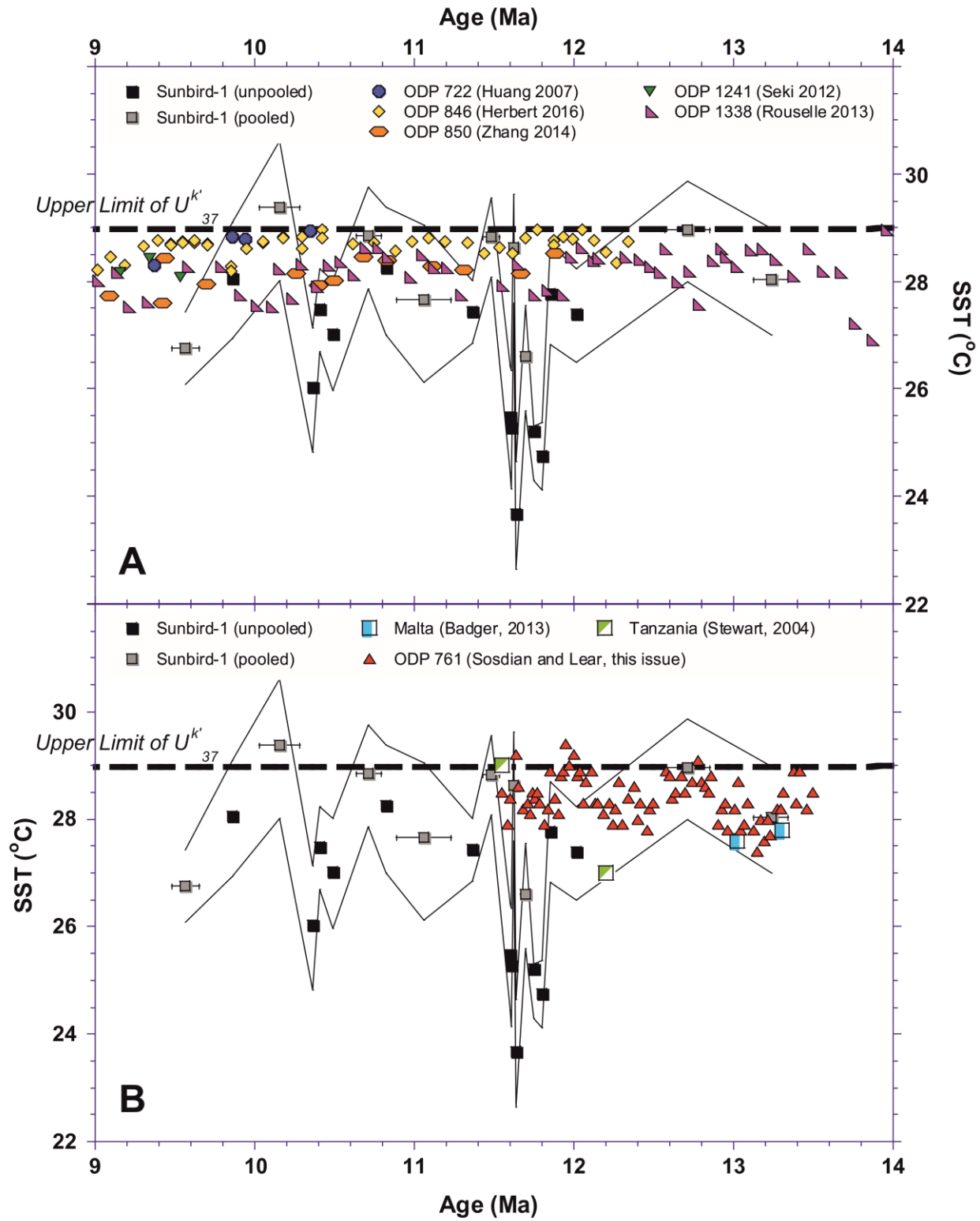
490 4.1 Reconstructing sea surface temperature from diagenetically altered foraminifera using
 491 laser ablation ICP-MS

492 Robust paleotemperature reconstructions using foraminiferal Mg/Ca ratios are reliant
 493 upon the Mg/Ca ratio recording a primary environmental signal, unaltered by diagenetic
 494 alteration. Despite employing a thorough cleaning protocol (*Barker et al.*, 2003; *Boyle and*
 495 *Keigwin*, 1985), our Mg/Ca ratios from solution-based ICP-MS analysis in the >11.8 Ma portion
 496 of the record are clearly influenced by a diagenetic contaminant phase containing elevated
 497 magnesium (Figure 4). The application of LA-ICP-MS to collect high resolution elemental
 498 profiles through the foraminiferal tests, excluding regions displaying diagenetic contamination,
 499 has facilitated the identification of what we interpret to be primary paleotemperatures from
 500 diagenetically altered foraminifera (*Hines et al.*, 2017; *Hollis et al.*, 2015).
 501

502 The Sunbird-1 $\delta^{18}\text{O}_{\text{PF}}$ SST record from *G. obliquus* reconstructs very similar absolute
 503 temperatures to the planktic foraminiferal Mg/Ca SST record (Figure 7c, Supplementary Table
 504 S8 and S9). Mean SST from the Sunbird-1 $\delta^{18}\text{O}_{\text{PF}}$ record (29°C) is 2°C higher than mean SST
 505 from the Mg/Ca record (27°C), although with the exception of the two transient decreases in
 506 Mg/Ca reconstructed SST initiating at 11.8 Ma and 10.7 Ma the records are within error. The
 507 similarity of the absolute SSTs reconstructed by the two proxies, strengthens the case for the LA-
 508 ICP-MS Mg/Ca SST record recording a primary temperature signal and that these absolute sea
 509 surface temperatures at Sunbird-1 should be considered primary.

510 4.2 Mid-late Miocene sea surface temperatures in the equatorial Indian Ocean

511 The results from Sunbird-1 indicate that SST in the equatorial Indian Ocean remained
 512 stable at ~27°C-29°C through the 13.3 Ma to 9.5 Ma interval (Figure 7c). This suggests that
 513 tropical climate was relatively stable following the global cooling associated with the expansion
 514 of the East Antarctic Ice Sheet across the MMCT. These records from Sunbird-1 supports the
 515 robustness of contemporaneous alkenone based studies which exhibit similar absolute tropical
 516 SST estimates (*Herbert et al.*, 2016; *Huang et al.*, 2007; *Rousselle et al.*, 2013; *Seki et al.*, 2012;
 517 *Zhang et al.*, 2014) (Figure 8a). The U_{37}^{k} SST calibration fails to reconstruct SST >29°C (*Müller*
 518 *et al.*, 1998) but these results using Mg/Ca paleo-thermometry suggest that this restriction does
 519 not apply to this time interval, unlike the preceding Miocene Climatic Optimum during which
 520 Mg/Ca temperature estimates are higher than those estimated with the U_{37}^{k} proxy (*Badger et al.*,
 521 2013).



523 **Figure 8:** LA-ICP-MS derived SST at Sunbird-1 compared to and SST estimates at
 524 contemporaneous sites from (a) U_{37}^k , and (b) foraminiferal geochemistry. Estimates applying U_{37}^k
 525 are from ODP Site 722 (*Huang et al.*, 2007) in the Arabian Sea, and ODP & IODP Sites 846
 526 (*Herbert et al.*, 2016), 850 (*Zhang et al.*, 2014), 1241 (*Seki et al.*, 2012), and U1338 (*Rousselle et*
 527 *al.*, 2013) in the Eastern Equatorial Pacific. Estimates applying the foraminiferal Mg/Ca proxy
 528 are from ODP Sites 761 (*Sosdian and Lear*, this issue) and terrestrial outcrops in Malta (*Badger*
 529 *et al.*, 2013). Two temperature estimates using the $\delta^{18}O$ of exceptionally preserved foraminifera
 530 from Tanzania are also shown (*Stewart et al.*, 2004). The upper limit for the U_{37}^k proxy (29°C) is
 531 marked by the thick dashed black line. All previously published records used for comparison are
 532 kept on their original age models.

533
 534
 535

536 Although not a true tropical location, and only two data points, the *Badger et al.* (2013)
 537 Mg/Ca record from the Mediterranean estimates SST of ~27.5°C at ~13 Ma, both within the
 538 Sunbird-1 SST uncertainty envelope (Figure 8b). Mg/Ca-SST records based on less well-
 539 preserved planktic foraminifera also suggest stable tropical SST of 27-29°C between 13.8 and
 540 11.4 Ma (*Sosdian and Lear*, this issue) (Figure 8b). This suggests that planktic foraminiferal
 541 Mg/Ca may be relatively robust to diagenetic recrystallization processes. Furthermore, well
 542 preserved planktic foraminifera from clay-rich sediments of coastal Tanzania yield Indian Ocean
 543 sea surface temperatures of 27°C at 12.2 Ma and 29°C at 11.55 Ma using the $\delta^{18}O$ paleo-
 544 thermometer (*Stewart et al.*, 2004), again in agreement with the Sunbird-1 temperature estimates
 545 (Figure 8b). Although sparse in number, previous absolute tropical SST estimates are in
 546 agreement with those reconstructed from Sunbird-1. It is worth noting that this study, as well as
 547 the tropical SST records of *Herbert et al.* (2016) and references therein, do not sample the warm
 548 pool of the Western Pacific, where we would expect SST to be greater than 29°C, temperatures
 549 which unsaturated alkenones cannot reconstruct.

550

551 Although the improved estimates provided by the Sunbird-1 record suggest absolute
 552 tropical sea surface temperatures remained relatively stable through the mid-late Miocene some
 553 temporal variability does persist. Between 11.8 Ma and 11.7 Ma SST drops sharply by ~3°C.
 554 Excluding one value of 28.6°C at 11.62 Ma, this decrease in SST to ~24-25°C persists for ~300
 555 kyr before recovering to pre excursion values by 11.5 Ma. However, no transient decrease in sea
 556 surface temperature is recorded from contemporaneous alkenone based estimates of tropical SST
 557 utilizing the U_{37}^k proxy from the Arabian Sea (*Huang et al.*, 2007), and the Eastern Equatorial
 558 Pacific (*Herbert et al.*, 2016; *Rousselle et al.*, 2013; *Seki et al.*, 2012; *Zhang et al.*, 2014) (Figure
 559 8a). This suggests that this observed transient ~3°C SST decrease is not the result of a global
 560 driver, and supports a mechanism causing local ocean cooling of the surface waters at Sunbird-1.
 561 An alternative hypothesis is that an unaccounted increase in local salinity and/or pH, lowering
 562 foraminiferal Mg/Ca ratios, caused a bias to cooler temperatures between ~11.8 and 11.5 Ma.
 563 The planktic $\delta^{18}O$ record does not support a significant change in sea surface salinity at this time
 564 (Figure 7c). Despite incorporating varying pH from a globally distributed set of open ocean sites
 565 (*Sosdian et al.*, 2018), any localized changes in pH at Sunbird-1 cannot be accounted for. This

566 may be particularly relevant considering the land-proximal, tectonically active nature of the
567 study site. However, our preferred interpretation is for a local cooling between ~11.8 and 11.5
568 Ma. The lack of a marked increase in the planktic $\delta^{18}\text{O}$ record at this time implies that the
569 cooling was associated with a freshening of surface waters (Figure 7c). Interestingly, this interval
570 corresponds to a period of very high sedimentation rates (Figure S1), which might be consistent
571 with enhanced precipitation and runoff, lowering regional surface salinity.
572

573 4.3 Implications for the global climate state during the mid-late Miocene

574 Previous studies, utilizing the U_{37}^k proxy suggest a substantial cooling of sea surface
575 temperature at mid-to-high latitudes in both hemispheres between 10 and 5.5 Ma, whilst tropical
576 sea surface temperatures show limited cooling in the late Miocene prior to ~7 Ma (*Herbert et al.*,
577 2016; *LaRiviere et al.*, 2012). The absolute tropical SST record reported in this study supports
578 the finding that the latitudinal temperature gradient steepened in the late Miocene, as the climate
579 system transitioned towards its modern-day state. Furthermore, support for the absolute
580 temperatures reconstructed by the alkenone proxy suggests that the interval between 10 and 7.5
581 Ma was associated with enhanced polar amplification, significantly greater than that calculated
582 for the greenhouse climate of the Eocene (*Cramwinckel et al.*, 2018). There is little evidence for
583 a significant change in $p\text{CO}_2$ in this interval (*Sosdian et al.*, 2018; *Stoll et al.*, 2019). We
584 speculate that the marked regional cooling between 10 and 7.5 Ma perhaps reflects processes
585 internal to the climate system, involving for example ocean-atmospheric heat transport, sea ice
586 extent, or changes in regional cloud cover. A combined data-modelling approach would help
587 constrain possible factors and explore potential relationships between this highly heterogeneous
588 cooling and the CO_2 drawdown that was associated with the subsequent global late Miocene
589 Cooling.
590

591 5 Conclusions

592 Our Sunbird-1 sea surface temperature estimates from LA-ICP-MS Mg/Ca analyses are
593 in good agreement with those using the $\delta^{18}\text{O}$ paleo-thermometer on glassy foraminifera,
594 supporting the use of LA-ICP-MS micro-analysis across multiple specimens for reconstructing
595 paleotemperatures. This analytical technique has allowed the reconstruction of reliable Mg/Ca
596 derived palaeotemperatures using foraminifera whose bulk trace element ratios demonstrate
597 diagenetic contamination by authigenic coatings. This opens the potential for Mg/Ca
598 paleothermometry on other challenging time intervals, and locations, where contaminant
599 coatings have previously inhibited the geochemical analysis of primary foraminiferal calcite. We
600 present new, absolute sea surface temperature records from planktic foraminiferal Mg/Ca for the
601 south west Indian Ocean between 13.5 Ma and 9.5 Ma. Absolute estimates of 24-31°C suggest
602 that sea surface temperature was relatively constant through the interval, although our record also
603 suggests two intervals of regional cooling and freshening of surface waters at 11.8 and 10.7 Ma.
604 The late Miocene represented a key interval in the transition of Earth's climate to its modern
605 state, including the development of stronger latitudinal temperature gradients. Our new
606 temperature record suggests different mechanisms may have been responsible for this cooling.
607 The initial cooling from ~10 Ma at mid to high latitudes in both hemispheres was not associated
608 with significant cooling at low latitudes. On the other hand, the late Miocene cooling between

609 ~7.5 and 5.5 Ma was global in nature and associated with a drawdown in pCO₂. Further work
 610 should therefore explore the possibility of carbon cycle feedbacks in determining the full
 611 magnitude of the late Miocene Cooling.

612

613 **Acknowledgments, Samples, and Data**

614 This study uses samples from the Sunbird-1 core provided by BG-Group. Data can be found in
 615 Supplementary Tables S1 to S9 of the supporting information, and will be uploaded to the online
 616 database Pangaea. We thank Alexandra Nederbragt and Anabel Morte-Rodeñas for laboratory
 617 assistance. We thank the reviewers and editor for their insightful comments that improved the
 618 manuscript. This research was supported by NERC iCASE studentship BW/22003105 (M.G.N.),
 619 and NE/L009633/1 grant to C.H.L.

620

621

622

623 **References**

- 624 Anand, P., Elderfield, H., & Conte, M. H. (2003). Calibration of Mg/Ca thermometry in planktonic foraminifera
 625 from a sediment trap time series. *Paleoceanography*, *18*(2). <https://doi.org/10.1029/2002PA000846>
- 626 Aze, T., Ezard, T. H., Purvis, A., Coxall, H. K., Stewart, D. R., Wade, B. S., & Pearson, P. N. (2011). A phylogeny
 627 of Cenozoic macroperforate planktonic foraminifera from fossil data. *Biological Reviews*, *86*(4), 900-927.
 628 <https://doi.org/10.1111/j.1469-185X.2011.00178.x>
- 629 Backman, J., Raffi, I., Rio, D., Fornaciari, E., & Pälike, H. (2012). Biozonation and biochronology of Miocene
 630 through Pleistocene calcareous nannofossils from low and middle latitudes. *Newsletters on Stratigraphy*,
 631 *45*(3), 221-244. 10.1127/0078-0421/2012/0022
- 632 Badger, M. P., Lear, C. H., Pancost, R. D., Foster, G. L., Bailey, T. R., Leng, M. J., & Abels, H. A. (2013). CO₂
 633 drawdown following the middle Miocene expansion of the Antarctic Ice Sheet. *Paleoceanography*, *28*(1),
 634 42-53. <https://doi.org/10.1002/palo.20015>
- 635 Barker, S., Greaves, M., & Elderfield, H. (2003). A study of cleaning procedures used for foraminiferal Mg/Ca
 636 paleothermometry. *Geochemistry, Geophysics, Geosystems*, *4*(9). <https://doi.org/10.1029/2003GC000559>
- 637 Bemis, B. E., Spero, H. J., Bijma, J., & Lea, D. W. (1998). Reevaluation of the oxygen isotopic composition of
 638 planktonic foraminifera: Experimental results and revised paleotemperature equations. *Paleoceanography*,
 639 *13*(2), 150-160. <https://doi.org/10.1029/98PA00070>
- 640 Bertlich, J., Nürnberg, D., Hathorne, E. C., De Nooijer, L. J., Mezger, E. M., Kienast, M., et al. (2018). Salinity
 641 control on Na incorporation into calcite tests of the planktonic foraminifera *Trilobatus sacculifer*—evidence
 642 from culture experiments and surface sediments. *Biogeosciences (BG)*, *15*(20), 5991-6018.
 643 <http://dx.doi.org/10.5194/bg-2018-164>
- 644 Boyer, T. P., Antonov, J. I., Baranova, O. K., Coleman, C., Garcia, H. E., Grodsky, A., et al. (2013). World Ocean
 645 Database 2013.
- 646 Boyle, E., & Keigwin, L. (1985). Comparison of Atlantic and Pacific paleochemical records for the last 215,000
 647 years: Changes in deep ocean circulation and chemical inventories. *Earth and Planetary Science Letters*,
 648 *76*(1), 135-150. [http://doi.org/0012-821x/85/\\$03.30](http://doi.org/0012-821x/85/$03.30)
- 649 Boyle, E. A. (1983). Manganese carbonate overgrowths on foraminifera tests. *Geochimica et Cosmochimica Acta*,
 650 *47*(10), 1815-1819. [https://doi.org/10.1016/0016-7037\(83\)90029-7](https://doi.org/10.1016/0016-7037(83)90029-7)
- 651 Broecker, W. S., Peng, T.-H., & Beng, Z. (1982). *Tracers in the Sea*: Lamont-Doherty Geological Observatory,
 652 Columbia University.

- 653 Chen, P., Yu, J., & Jin, Z. (2017). An evaluation of benthic foraminiferal U/Ca and U/Mn proxies for deep ocean
654 carbonate chemistry and redox conditions. *Geochemistry, Geophysics, Geosystems*. Article in Press.
655 <http://doi.org/10.1002/2016GC006730>
- 656 Coggon, R. M., Teagle, D. A., Smith-Duque, C. E., Alt, J. C., & Cooper, M. J. (2010). Reconstructing past seawater
657 Mg/Ca and Sr/Ca from mid-ocean ridge flank calcium carbonate veins. *Science*, 327(5969), 1114-1117.
658 <http://doi.org/10.1126/science.1182252>
- 659 Cramer, B., Miller, K., Barrett, P., & Wright, J. (2011). Late Cretaceous–Neogene trends in deep ocean temperature
660 and continental ice volume: reconciling records of benthic foraminiferal geochemistry ($\delta^{18}\text{O}$ and Mg/Ca)
661 with sea level history. *Journal of Geophysical Research: Oceans* (1978–2012), 116(C12).
662 <https://doi.org/10.1029/2011JC007255>
- 663 Cramwinckel, M. J., Huber, M., Kocken, I. J., Agnini, C., Bijl, P. K., Bohaty, S. M., et al. (2018). Synchronous
664 tropical and polar temperature evolution in the Eocene. *Nature*, 559(7714), 382-386.
665 <http://doi.org/10.1038/s41586-018-0272-2>
- 666 Creech, J. B., Baker, J. A., Hollis, C. J., Morgans, H. E. G., & Smith, E. G. C. (2010). Eocene sea temperatures for
667 the mid-latitude southwest Pacific from Mg/Ca ratios in planktonic and benthic foraminifera. *Earth and
668 Planetary Science Letters*, 299(3–4), 483-495. <http://dx.doi.org/10.1016/j.epsl.2010.09.039>
- 669 de Nooijer, L. J., Hathorne, E. C., Reichart, G.-J., Langer, G., & Bijma, J. (2014). Variability in calcitic Mg/Ca and
670 Sr/Ca ratios in clones of the benthic foraminifer *Ammonia tepida*. *Marine Micropaleontology*, 107, 32-43.
671 <https://doi.org/10.1016/j.marmicro.2014.02.002>
- 672 de Nooijer, L. J., van Dijk, I., Toyofuku, T., & Reichart, G. J. (2017). The Impacts of Seawater Mg/Ca and
673 Temperature on Element Incorporation in Benthic Foraminiferal Calcite. *Geochemistry, Geophysics,
674 Geosystems*, 18(10), 3617-3630. <http://doi.org/10.1002/2017GC007183>
- 675 Detlef, H., Sosdian, S. M., Kender, S., Lear, C. H., & Hall, I. R. (2019). Multi-elemental composition of authigenic
676 carbonates in benthic foraminifera from the eastern Bering Sea continental margin (International Ocean
677 Discovery Program Site U1343). *Geochimica et Cosmochimica Acta*.
678 <https://doi.org/10.1016/j.gca.2019.09.025>
- 679 Dickson, J. A. D. (2002). Fossil Echinoderms As Monitor of the Mg/Ca Ratio of Phanerozoic Oceans. *Science*,
680 298(5596), 1222-1224. <http://doi.org/10.1126/science.1075882>
- 681 Eggins, S., De Deckker, P., & Marshall, J. (2003). Mg/Ca variation in planktonic foraminifera tests: implications for
682 reconstructing palaeo-seawater temperature and habitat migration. *Earth and Planetary Science Letters*,
683 212(3), 291-306. [https://doi.org/10.1016/S0012-821X\(03\)00283-8](https://doi.org/10.1016/S0012-821X(03)00283-8)
- 684 Eggins, S. M., Sadekov, A., & De Deckker, P. (2004). Modulation and daily banding of Mg/Ca in *Orbulina universa*
685 tests by symbiont photosynthesis and respiration: a complication for seawater thermometry? *Earth and
686 Planetary Science Letters*, 225(3), 411-419. <https://doi.org/10.1016/j.epsl.2004.06.019>
- 687 Evans, D., Bhatia, R., Stoll, H., & Müller, W. (2015). LA-ICPMS Ba/Ca analyses of planktic foraminifera from the
688 Bay of Bengal: Implications for late Pleistocene orbital control on monsoon freshwater flux. *Geochemistry,
689 Geophysics, Geosystems*, 16(8), 2598-2618. <https://doi.org/10.1002/2015GC005822>
- 690 Evans, D., Brierley, C., Raymo, M. E., Erez, J., & Müller, W. (2016). Planktic foraminifera shell chemistry response
691 to seawater chemistry: Pliocene-Pleistocene seawater Mg/Ca, temperature and sea level change. *Earth and
692 Planetary Science Letters*. Article in Press. <http://doi.org/10.1016/j.epsl.2016.01.013>
- 693 Evans, D., & Müller, W. (2018). Automated Extraction of a Five-Year LA-ICP-MS Trace Element Dataset of Ten
694 Common Glass and Carbonate Reference Materials: Long-Term Data Quality, Optimisation and Laser Cell
695 Homogeneity. *Geostandards and Geoanalytical Research*. <https://doi.org/10.1111/ggr.12204>
- 696 Evans, D., Sagoo, N., Renema, W., Cotton, L. J., Müller, W., Todd, J. A., et al. (2018). Eocene greenhouse climate
697 revealed by coupled clumped isotope-Mg/Ca thermometry. *Proceedings of the National Academy of
698 Sciences of the United States of America*, 115(6), 1174-1179. Article.
699 <http://doi.org/10.1073/pnas.1714744115>
- 700 Evans, D., Wade, B. S., Henahan, M., Erez, J., & Müller, W. (2016). Revisiting carbonate chemistry controls on
701 planktic foraminifera Mg / Ca: Implications for sea surface temperature and hydrology shifts over the
702 Paleocene-Eocene Thermal Maximum and Eocene-Oligocene transition. *Climate of the Past*, 12(4), 819-
703 835. Article. <http://doi.org/10.5194/cp-12-819-2016>
- 704 Farrell, J. W., Raffi, I., Janecek, T. R., Murray, D. W., Levitan, M., Dadey, K. A., et al. (1995). 35. LATE
705 NEOGENE SEDIMENTATION PATTERNS IN THE EASTERN EQUATORIAL PACIFIC OCEAN1.
- 706 Fehrenbacher, J. S., & Martin, P. A. (2014). Exploring the dissolution effect on the intrashell Mg/Ca variability of
707 the planktic foraminifer *Globigerinoides ruber*. *Paleoceanography*, 29(9), 854-868.
708 <https://doi.org/10.1002/2013PA002571>

- 709 Fehrenbacher, J. S., Spero, H. J., Russell, A. D., Vetter, L., & Eggins, S. (2015). Optimizing LA-ICP-MS analytical
710 procedures for elemental depth profiling of foraminifera shells. *Chemical Geology*, 407-408, 2-9.
711 <http://doi.org/10.1016/j.chemgeo.2015.04.007>
- 712 Foster, G. L., Lear, C. H., & Rae, J. W. B. (2012). The evolution of pCO₂, ice volume and climate during the middle
713 Miocene. *Earth and Planetary Science Letters*, 341-344(0), 243-254.
714 <http://dx.doi.org/10.1016/j.epsl.2012.06.007>
- 715 Foster, G. L., & Rae, J. W. (2015). Reconstructing Ocean pH with Boron Isotopes in Foraminifera. *Annual Review*
716 *of Earth and Planetary Sciences*(0). [https://www.annualreviews.org/doi/full/10.1146/annurev-earth-](https://www.annualreviews.org/doi/full/10.1146/annurev-earth-060115-012226#_i63)
717 [060115-012226#_i63](https://www.annualreviews.org/doi/full/10.1146/annurev-earth-060115-012226#_i63)
- 718 Geerken, E., De Nooijer, L. J., Van Dijk, I., & Reichart, G.-J. (2018). Impact of salinity on element incorporation in
719 two benthic foraminiferal species with contrasting magnesium contents. *Biogeosciences*, 15(7), 2205-2218.
720 <https://doi.org/10.5194/bg-15-2205-2018>
- 721 Gradstein, F. M., Ogg, J. G., & Smith, A. G. (2004). *A geologic time scale 2004* (Vol. 86): Cambridge University
722 Press.
- 723 Gray, W. R., & Evans, D. (2019). Nonthermal influences on Mg/Ca in planktonic foraminifera: a review of culture
724 studies and application to the Last Glacial Maximum. *Paleoceanography and Paleoclimatology*, 34(3),
725 306-315. <https://doi.org/10.1029/2018PA003517>
- 726 Gray, W. R., Weldeab, S., Lea, D. W., Rosenthal, Y., Gruber, N., Donner, B., & Fischer, G. (2018). The effects of
727 temperature, salinity, and the carbonate system on Mg/Ca in Globigerinoides ruber (white): A global
728 sediment trap calibration. *Earth and Planetary Science Letters*, 482, 607-620. Article.
729 <http://doi.org/10.1016/j.epsl.2017.11.026>
- 730 Greenop, R., Foster, G. L., Wilson, P. A., & Lear, C. H. (2014). Middle Miocene climate instability associated with
731 high-amplitude CO₂ variability. *Paleoceanography*, 29(9), 845-853.
732 <https://doi.org/10.1002/2014PA002653>
- 733 Greenop, R., Hain, M. P., Sosdian, S. M., Oliver, K. I. C., Goodwin, P., Chalk, T. B., et al. (2017). A record of
734 Neogene seawater δ¹¹B reconstructed from paired δ¹¹B analyses on benthic and planktic foraminifera.
735 *Climate of the Past*, 13(2), 149-170. Article. <https://doi.org/10.5194/cp-13-149-2017>
- 736 Guillong, M., L. Meier, D., Allan, M., A. Heinrich, C., & Yardley, B. (2008). *SILLS: A MATLAB-based program for*
737 *the reduction of laser ablation ICP-MS data of homogeneous materials and inclusions* (Vol. 40).
- 738 Hasenfratz, A. P., Martínez-García, A., Jaccard, S. L., Vance, D., Wälle, M., Greaves, M., & Haug, G. H. (2016).
739 Determination of the Mg/Mn ratio in foraminiferal coatings: An approach to correct Mg/Ca temperatures
740 for Mn-rich contaminant phases. *Earth and Planetary Science Letters*.
741 <http://dx.doi.org/10.1016/j.epsl.2016.10.004>
- 742 Henehan, M. J., Rae, J. W. B., Foster, G. L., Erez, J., Prentice, K. C., Kucera, M., et al. (2013). Calibration of the
743 boron isotope proxy in the planktonic foraminifera Globigerinoides ruber for use in palaeo-CO₂
744 reconstruction. *Earth and Planetary Science Letters*, 364, 111-122.
745 <https://doi.org/10.1016/j.epsl.2012.12.029>
- 746 Herbert, T. D., Lawrence, K. T., Tzanova, A., Peterson, L. C., Caballero-Gill, R., & Kelly, C. S. (2016). Late
747 Miocene global cooling and the rise of modern ecosystems. *Nature Geoscience*.
748 <https://doi.org/10.1038/ngeo2813>
- 749 Hines, B. R., Hollis, C. J., Atkins, C. B., Baker, J. A., Morgans, H. E. G., & Strong, P. C. (2017). Reduction of
750 oceanic temperature gradients in the early Eocene Southwest Pacific Ocean. *Palaeogeography,*
751 *Palaeoclimatology, Palaeoecology*, 475, 41-54. <https://doi.org/10.1016/j.palaeo.2017.02.037>
- 752 Holland, K., Branson, O., Haynes, L. L., Hönisch, B., Allen, K. A., Russell, A. D., et al. (2020). Constraining
753 multiple controls on planktic foraminifera Mg/Ca. *Geochimica et Cosmochimica Acta*, 273, 116-136.
754 Article. <https://doi.org/10.1016/j.gca.2020.01.015>
- 755 Hollis, C., Dunkley Jones, T., Anagnostou, E., Bijl, P., Cramwinckel, M., Cui, Y., et al. (2019). The DeepMIP
756 contribution to PMIP4: methodologies for selection, compilation and analysis of latest Paleocene and early
757 Eocene climate proxy data, incorporating version 0.1 of the DeepMIP database. *Geoscientific Model*
758 *Development Discussions*, 2019, 1-98. <http://dx.doi.org/10.5194/gmd-12-3149-2019>
- 759 Hollis, C., Hines, B., Littler, K., Villasante-Marcos, V., Kulhanek, D., Strong, C., et al. (2015). The Paleocene–
760 Eocene Thermal Maximum at DSDP Site 277, Campbell Plateau, southern Pacific Ocean.
761 <https://doi.org/10.5194/cp-11-1009-2015>
- 762 Hönisch, B., Allen, K. A., Lea, D. W., Spero, H. J., Eggins, S. M., Arbuszewski, J., et al. (2013). The influence of
763 salinity on Mg/Ca in planktic foraminifera—Evidence from cultures, core-top sediments and complementary
764 δ¹⁸O. *Geochimica et Cosmochimica Acta*, 121, 196-213. <https://doi.org/10.1016/j.gca.2013.07.028>

- 765 Horita, J., Zimmermann, H., & Holland, H. D. (2002). Chemical evolution of seawater during the Phanerozoic:
766 Implications from the record of marine evaporites. *Geochimica et Cosmochimica Acta*, 66(21), 3733-3756.
767 [https://doi.org/10.1016/S0016-7037\(01\)00884-5](https://doi.org/10.1016/S0016-7037(01)00884-5)
- 768 Huang, Y., Clemens, S. C., Liu, W., Wang, Y., & Prell, W. L. (2007). Large-scale hydrological change drove the
769 late Miocene C4 plant expansion in the Himalayan foreland and Arabian Peninsula. *Geology*, 35(6), 531-
770 534. <https://doi.org/10.1130/G23666A.1>
- 771 Hut, G. (1987). Consultants' group meeting on stable isotope reference samples for geochemical and hydrological
772 investigations.
- 773 Jiang, S., Wise, S., & Wang, Y. (2007). *Cause of the middle/late Miocene carbonate crash: dissolution or low*
774 *productivity*. Paper presented at the Proceedings of the Ocean Drilling Program. Scientific Results.
- 775 Jochum, K. P., Weis, U., Stoll, B., Kuzmin, D., Yang, Q., Raczek, I., et al. (2011). Determination of reference
776 values for NIST SRM 610–617 glasses following ISO guidelines. *Geostandards and Geoanalytical*
777 *Research*, 35(4), 397-429. <https://doi.org/10.1111/j.1751-908X.2011.00120.x>
- 778 Keller, G. (1985). Depth stratification of planktonic foraminifers in the Miocene ocean. *The Miocene ocean:*
779 *paleoceanography and biogeography*, 163, 177-196.
- 780 Keller, G., & Barron, J. A. (1987). Paleodepth distribution of Neocene deep-sea hiatuses. *Paleoceanography*, 2(6),
781 697-713. <https://doi.org/10.1029/PA002i006p00697>
- 782 Kısakürek, B., Eisenhauer, A., Böhm, F., Garbe-Schönberg, D., & Erez, J. (2008). Controls on shell Mg/Ca and
783 Sr/Ca in cultured planktonic foraminiferan, *Globigerinoides ruber* (white). *Earth and Planetary Science*
784 *Letters*, 273(3-4), 260-269. <https://doi.org/10.1016/j.epsl.2008.06.026>
- 785 Knorr, G., Butzin, M., Micheels, A., & Lohmann, G. (2011). A warm Miocene climate at low atmospheric CO₂
786 levels. *Geophysical Research Letters*, 38(20). <https://doi.org/10.1029/2011GL048873>
- 787 Koho, K., de Nooijer, L., & Reichert, G. (2015). Combining benthic foraminiferal ecology and shell Mn/Ca to
788 deconvolve past bottom water oxygenation and paleoproductivity. *Geochimica et Cosmochimica Acta*, 165,
789 294-306. <https://doi.org/10.1016/j.gca.2015.06.003>
- 790 LaRiviere, J. P., Ravelo, A. C., Crimmins, A., Dekens, P. S., Ford, H. L., Lyle, M., & Wara, M. W. (2012). Late
791 Miocene decoupling of oceanic warmth and atmospheric carbon dioxide forcing. *Nature*, 486(7401), 97.
792 <https://doi.org/10.1038/nature11200>
- 793 Lear, C. H., Coxall, H. K., Foster, G. L., Lunt, D. J., Mawbey, E. M., Rosenthal, Y., et al. (2015). Neogene ice
794 volume and ocean temperatures: Insights from infaunal foraminiferal Mg/Ca paleothermometry.
795 *Paleoceanography*. <https://doi.org/10.1002/2015PA002833>
- 796 Lear, C. H., Mawbey, E. M., & Rosenthal, Y. (2010). Cenozoic benthic foraminiferal Mg/Ca and Li/Ca records:
797 Toward unlocking temperatures and saturation states. *Paleoceanography*, 25(4).
798 <https://doi.org/10.1029/2009pa001880>
- 799 Lear, C. H., Rosenthal, Y., & Slowey, N. (2002). Benthic foraminiferal Mg/Ca-paleothermometry: A revised core-
800 top calibration. *Geochimica et Cosmochimica Acta*, 66(19), 3375-3387. [https://doi.org/10.1016/S0016-](https://doi.org/10.1016/S0016-7037(02)00941-9)
801 [7037\(02\)00941-9](https://doi.org/10.1016/S0016-7037(02)00941-9)
- 802 LeGrande, A. N., & Schmidt, G. A. (2006). Global gridded data set of the oxygen isotopic composition in seawater.
803 *Geophysical Research Letters*, 33(12). <https://doi.org/10.1029/2006GL026011>
- 804 Lemarchand, D., Gaillardet, J., Lewin, E., & Allegre, C. (2002). Boron isotope systematics in large rivers:
805 implications for the marine boron budget and paleo-pH reconstruction over the Cenozoic. *Chemical*
806 *Geology*, 190(1), 123-140. [https://doi.org/10.1016/S0009-2541\(02\)00114-6](https://doi.org/10.1016/S0009-2541(02)00114-6)
- 807 Longerich, H. P., Jackson, S. E., & Günther, D. (1996). Inter-laboratory note. Laser ablation inductively coupled
808 plasma mass spectrometric transient signal data acquisition and analyte concentration calculation. *Journal*
809 *of analytical atomic spectrometry*, 11(9), 899-904. <https://doi.org/10.1039/JA9961100899>
- 810 Lübbers, J., Kuhnt, W., Holbourn, A. E., Bolton, C. T., Gray, E., Usui, Y., et al. (2019). The middle to late Miocene
811 “Carbonate Crash” in the equatorial Indian Ocean. *Paleoceanography and Paleoclimatology*, 34(5), 813-
812 832. <https://doi.org/10.1029/2018PA003482>
- 813 Lunt, D. J., Flecker, R., Valdes, P. J., Salzmann, U., Gladstone, R., & Haywood, A. M. (2008). A methodology for
814 targeting palaeo proxy data acquisition: A case study for the terrestrial late Miocene. *Earth and Planetary*
815 *Science Letters*, 271(1), 53-62. <https://doi.org/10.1016/j.epsl.2008.03.035>
- 816 Lyle, M., Dadey, K. A., & Farrell, J. W. (1995). 42. The Late Miocene (11–8 Ma) Eastern Pacific Carbonate Crash:
817 evidence for reorganization of deep-water Circulation by the closure of the Panama Gateway. *1995*
818 *Proceedings of the Ocean Drilling Program, Scientific Results*, 138.

- 819 Mayk, D., Fietzke, J., Anagnostou, E., & Paytan, A. (2020). LA-MC-ICP-MS study of boron isotopes in individual
820 planktonic foraminifera: A novel approach to obtain seasonal variability patterns. *Chemical Geology*, 531.
821 Article. <https://doi.org/10.1016/j.chemgeo.2019.119351>
- 822 Müller, P. J., Kirst, G., Ruhland, G., Von Storch, I., & Rosell-Melé, A. (1998). Calibration of the alkenone
823 paleotemperature index U 37 K' based on core-tops from the eastern South Atlantic and the global ocean
824 (60 N-60 S). *Geochimica et Cosmochimica Acta*, 62(10), 1757-1772. [https://doi.org/10.1016/S0016-7037\(98\)00097-0](https://doi.org/10.1016/S0016-7037(98)00097-0)
- 825
- 826 Nairn, M. (2018). *Mid-Late Miocene climate constrained by a new Laser Ablation ICP-MS set up*. Cardiff
827 University,
- 828 Nürnberg, D., Bijma, J., & Hemleben, C. (1996). Assessing the reliability of magnesium in foraminiferal calcite as a
829 proxy for water mass temperatures. *Geochimica et Cosmochimica Acta*, 60(5), 803-814.
- 830 Pagani, M., Freeman, K. H., & Arthur, M. A. (1999). Late Miocene Atmospheric CO₂ Concentrations
831 and the Expansion of C₄ Grasses. *Science*, 285(5429), 876-879.
832 <https://doi.org/10.1126/science.285.5429.876>
- 833 Pearson, P. N., & Burgess, C. E. (2008). Foraminifer test preservation and diagenesis: comparison of high latitude
834 Eocene sites. *Geological Society, London, Special Publications*, 303(1), 59-72.
835 <https://doi.org/10.1144/SP303.5>
- 836 Pearson, P. N., Ditchfield, P. W., Singano, J., Harcourt-Brown, K. G., Nicholas, C. J., Olsson, R. K., et al. (2001).
837 Warm tropical sea surface temperatures in the Late Cretaceous and Eocene epochs. *Nature*, 413(6855),
838 481-487. <https://doi.org/10.1038/35097000>
- 839 Pena, L., Calvo, E., Cacho, I., Eggins, S., & Pelejero, C. (2005). Identification and removal of Mn-Mg-rich
840 contaminant phases on foraminiferal tests: Implications for Mg/Ca past temperature reconstructions.
841 *Geochemistry, Geophysics, Geosystems*, 6(9). <https://doi.org/10.1029/2005GC000930>
- 842 Petersen, J., Barras, C., Bézos, A., La, C., De Nooijer, L. J., Meysman, F. J. R., et al. (2018). Mn/Ca intra- and inter-
843 test variability in the benthic foraminifer *Ammonia tepida*. *Biogeosciences*, 15(1), 331-348. Article.
844 <https://doi.org/10.5194/bg-15-331-2018>
- 845 Piasias, N., & Mix, A. (1988). *Aliasing of the geologic record and the search for long-period Milankovitch cycles*
846 (Vol. 3).
- 847 Pound, M. J., Haywood, A. M., Salzmann, U., Riding, J. B., Lunt, D. J., & Hunter, S. J. (2011). A Tortonian (Late
848 Miocene, 11.61–7.25Ma) global vegetation reconstruction. *Palaeogeography, Palaeoclimatology,*
849 *Palaeoecology*, 300(1), 29-45. <https://doi.org/10.1016/j.palaeo.2010.11.029>
- 850 Raitzsch, M., & Hönisch, B. (2013). Cenozoic boron isotope variations in benthic foraminifers. *Geology*, 41(5), 591-
851 594. <https://doi.org/10.1130/g34031.1>
- 852 Raitzsch, M., Kuhnert, H., Hathorne, E. C., Groeneveld, J., & Bickert, T. (2011). U/Ca in benthic foraminifers: A
853 proxy for the deep-sea carbonate saturation. *Geochemistry, Geophysics, Geosystems*, 12(6).
854 <https://doi.org/10.1029/2010GC003344>
- 855 Rathmann, S., Hess, S., Kuhnert, H., & Mulitza, S. (2004). Mg/Ca ratios of the benthic foraminifera *Oridorsalis*
856 *umbonatus* obtained by laser ablation from core top sediments: Relationship to bottom water temperature.
857 *Geochemistry, Geophysics, Geosystems*, 5(12). <https://doi.org/10.1029/2004gc000808>
- 858 Reichart, G.-J., Jorissen, F., Anschutz, P., & Mason, P. R. (2003). Single foraminiferal test chemistry records the
859 marine environment. *Geology*, 31(4), 355-358. [https://doi.org/10.1130/0091-7613\(2003\)031<0355:SFTCRT>2.0.CO;2](https://doi.org/10.1130/0091-7613(2003)031<0355:SFTCRT>2.0.CO;2)
- 860
- 861 Rosenthal, Y., Boyle, E. A., & Slowey, N. (1997). Temperature control on the incorporation of magnesium,
862 strontium, fluorine, and cadmium into benthic foraminiferal shells from Little Bahama Bank: Prospects for
863 thermocline paleoceanography. *Geochimica et Cosmochimica Acta*, 61(17), 3633-3643.
- 864 Rousselle, G., Beltran, C., Sicre, M.-A., Raffi, I., & De Raféllis, M. (2013). Changes in sea-surface conditions in the
865 Equatorial Pacific during the middle Miocene–Pliocene as inferred from coccolith geochemistry. *Earth and*
866 *Planetary Science Letters*, 361, 412-421. <http://dx.doi.org/10.1016/j.epsl.2012.11.003>
- 867 Russell, A. D., Hönisch, B., Spero, H. J., & Lea, D. W. (2004). Effects of seawater carbonate ion concentration and
868 temperature on shell U, Mg, and Sr in cultured planktonic foraminifera. *Geochimica et Cosmochimica*
869 *Acta*, 68(21), 4347-4361. <https://doi.org/10.1016/j.gca.2004.03.013>
- 870 Sadekov, A., Eggins, S. M., De Deckker, P., & Kroon, D. (2008). Uncertainties in seawater thermometry deriving
871 from intratest and intertest Mg/Ca variability in *Globigerinoides ruber*. *Paleoceanography*, 23(1).
872 <https://doi.org/10.1029/2007pa001452>

- 873 Sadekov, A. Y., Eggins, S. M., & De Deckker, P. (2005). Characterization of Mg/Ca distributions in planktonic
874 foraminifera species by electron microprobe mapping. *Geochemistry, Geophysics, Geosystems*, 6(12).
875 <https://doi.org/10.1029/2005GC000973>
- 876 Schiebel, R., & Hemleben, C. (2017). *Planktic Foraminifers in the Modern Ocean*.
- 877 Schlitzer, R., Ocean Data View, odv.awi.de, (2018).
- 878 Seki, O., Schmidt, D., Schouten, S., C. Hopmans, E., Sinninghe-Damste, J., & D. Pancost, R. (2012).
879 *Paleoceanographic changes in the Eastern Equatorial Pacific over the last 10 Myr* (Vol. 27).
- 880 Sexton, P. F., Wilson, P. A., & Pearson, P. N. (2006). Microstructural and geochemical perspectives on planktic
881 foraminiferal preservation: “Glassy” versus “Frosty”. *Geochemistry, Geophysics, Geosystems*, 7(12).
882 <https://doi.org/10.1029/2006GC001291>
- 883 Sosdian, S. M., Greenop, R., Hain, M. P., Foster, G. L., Pearson, P. N., & Lear, C. H. (2018). Constraining the
884 evolution of Neogene ocean carbonate chemistry using the boron isotope pH proxy. *Earth and Planetary
885 Science Letters*, 498, 362-376. <https://doi.org/10.1016/j.epsl.2018.06.017>
- 886 Stewart, D. R. M., Pearson, P. N., Ditchfield, P. W., & Singano, J. M. (2004). Miocene tropical Indian Ocean
887 temperatures: evidence from three exceptionally preserved foraminiferal assemblages from Tanzania.
888 *Journal of African Earth Sciences*, 40(3), 173-189. <https://doi.org/10.1016/j.jafrearsci.2004.09.001>
- 889 Stoll, H. M., Guitian, J., Hernandez-Almeida, I., Mejia, L. M., Phelps, S., Polissar, P., et al. (2019). Upregulation of
890 phytoplankton carbon concentrating mechanisms during low CO₂ glacial periods and implications for the
891 phytoplankton pCO₂ proxy. *Quaternary Science Reviews*, 208, 1-20.
892 <https://doi.org/10.1016/j.quascirev.2019.01.012>
- 893 Super, J. R., Thomas, E., Pagani, M., Huber, M., O’Brien, C., & Hull, P. M. (2018). North Atlantic temperature and
894 p CO₂ coupling in the early-middle Miocene. *Geology*, 46(6), 519-522. <https://doi.org/10.1130/G40228.1>
- 895 Thil, F., Blamart, D., Assailly, C., Lazareth, C. E., Leblanc, T., Butsher, J., & Douville, E. (2016). Development of
896 laser ablation multi-collector inductively coupled plasma mass spectrometry for boron isotopic
897 measurement in marine biocarbonates: New improvements and application to a modern Porites coral. *Rapid
898 Communications in Mass Spectrometry*, 30(3), 359-371. Article. <https://doi.org/10.1002/rem.7448>
- 899 van Hinsbergen, D. J., de Groot, L. V., van Schaik, S. J., Spakman, W., Bijl, P. K., Sluijs, A., et al. (2015). A
900 paleolatitude calculator for paleoclimate studies. *PloS one*, 10(6).
901 <https://doi.org/DOI:10.1371/journal.pone.0126946>
- 902 Vetter, L., Kozdon, R., Mora, C. I., Eggins, S. M., Valley, J. W., Hönisch, B., & Spero, H. J. (2013). Micron-scale
903 intrashell oxygen isotope variation in cultured planktic foraminifers. *Geochimica et Cosmochimica Acta*,
904 107, 267-278. <https://doi.org/10.1016/j.gca.2012.12.046>
- 905 von der Heydt, A., & Dijkstra, H. A. (2006). Effect of ocean gateways on the global ocean circulation in the late
906 Oligocene and early Miocene. *Paleoceanography*, 21(1). <https://doi.org/10.1029/2005pa001149>
- 907 Wade, B. S., Pearson, P. N., Berggren, W. A., & Pälike, H. (2011). Review and revision of Cenozoic tropical
908 planktonic foraminiferal biostratigraphy and calibration to the geomagnetic polarity and astronomical time
909 scale. *Earth-Science Reviews*, 104(1), 111-142. <https://doi.org/10.1016/j.earscirev.2010.09.003>
- 910 Yu, J., & Elderfield, H. (2008). Mg/Ca in the benthic foraminifera *Cibicidoides wuellerstorfi* and *Cibicidoides mundulus*:
911 Temperature versus carbonate ion saturation. *Earth and Planetary Science
912 Letters*, 276(1), 129-139. <https://doi.org/10.1016/j.epsl.2008.09.015>
- 913 Zachos, J. C., Stott, L. D., & Lohmann, K. C. (1994). Evolution of early Cenozoic marine temperatures.
914 *Paleoceanography*, 9(2), 353-387. <https://doi.org/10.1029/93PA03266>
- 915 Zhang, Y. G., Pagani, M., & Liu, Z. (2014). A 12-Million-Year Temperature History of the Tropical Pacific Ocean.
916 *Science*, 344(6179), 84-87. <https://doi.org/10.1126/science.1246172>
- 917